JAY MONDAL

Novel Corrosion Protective Nanostructured Composite Coatings

JAY MONDAL

Novel Corrosion Protective Nanostructured Composite Coatings

The study was carried out in Department of Material Science, Institute of Physics, Faculty of Science and Technology, University of Tartu, Estonia

The Dissertation was admitted on February 8, 2016 in partial fulfilment of the requirements for the degree of Doctor of Philosophy in Material Science and allowed for defense by Scientific Council on Material Science of the Faculty of Science and Technology, University of Tartu.

Supervisor: Prof. Väino Sammelselg, Institute of Physics, Institute of
                Chemistry, University of Tartu, Tartu, Estonia

Opponents: Prof. Mário G. S. Ferreira, CICECO Aveiro Institute of Materials,
                University of Aveiro, Aveiro, Portugal

                Dr. Malle Krunks, Institute of Materials Science, Tallinn
                University of Technology, Tallinn, Estonia

Commencement: March 24, 2016 at the University of Tartu, Tartu, Estonia

University of Tartu Press
www.tyk.ee

CONTENTS

LIST OF ABBREVIATIONS

AFM	Atomic force microscope/microscopy
ALD	Atomic layer deposition
E_{corr}	Corrosion potential
EDX	Energy dispersive X-ray spectrometer/spectroscopy
EIS	Electrochemical impedance spectroscopy
E_{ocp}	Open circuit potential
E_{pit}	Pitting potential
FIB-SEM	Focused ion beam - scanning electron microscope/microscopy
FT-IR	Fourier transform infrared
GO	Graphene oxide
GO-PPy	Graphene oxide-polypyrrole hybrid
HR-SEM	High-resolution scanning electron microscope/microscopy
I_{corr}	Corrosion current density
I_{pass}	Passive current density
Laminate	Six ALD films: $3 \times (Al_2O_3/TiO_2)$
OM	Optical microscope/microscopy
rGO	Reduced graphene oxide
SS	Stainless steel (AISI 304)
Ti alloy	Titanium Ti-6Al-4V (grade 5) alloy
XRD	X-ray diffraction

LIST OF PUBLICATIONS

The thesis is based on the following papers:

I. **J. Mondal**, J. Kozlova, V. Sammelselg, Graphene Nanoplatelets Based Protective and Functionalizing Coatings for Stainless Steel, *J. Nanosci. Nanotechnol*. **15** (9) (2015) 6747–6750; DOI: 10.1166/jnn.2015.10774.

II. **J. Mondal**, M. Marandi, J. Kozlova, M. Merisalu, A. Niilisk, V. Sammelselg, Protection and Functionalizing of Stainless Steel Surface by Graphene oxide-Polypyrrole Composite Coating, *J. Chem. Chem. Eng*. **8** (2014) 786–793; .

III. **J. Mondal**, A. Marques, L. Aarik, J. Kozlova, A. Simões, V. Sammelselg, Development of a thin ceramic-graphene nanolaminate coating for corrosion protection of stainless steel, Corrosion Science (available online: 27.01.2016) DOI:10.1016/j.corsci.2016.01.013.

IV. **J. Mondal**, L. Aarik, J. Kozlova, A. Niilisk, H. Mändar, U. Mäeorg, A. Simões, V. Sammelselg. Functionalization of Titanium Alloy Surface by Graphene Nanoplatelets and Metal Oxides: Corrosion Inhibition, *J. Nanosci. Nanotechnol*. **15** (9) (2015) 6533-6540; DOI: 10.1166/ jnn.2015.10775.

List of other publications:

A. I. Kruusenberg, **J. Mondal**, L. Matisen, V. Sammelselg, K. Tammeveski, Oxygen reduction on graphene supported MN4 macromolecules in alkaline media. *Electrochem. Commun.* **33** (2013) 18–22; DOI: 10.1016/ j.elecom.2013.04.005.

B. K-K. Türk, I. Kruusenberg, **J. Mondal**, P. Rauwel, J. Kozlova, L. Matisen, V. Sammelselg, K. Tammeveski, Oxygen electroreduction on MN_4 macrocycle modified graphene/multi-walled carbon nanotube composites, *J. Electroanal. Chem,* **756** (2015) 69–76; DOI: 10.1016/ j.jelechem.2015.08.014)

C. H. Kwon, **J. Mondal**, K. AloGab, V. Sammelselg, M. Takamichi, A. Kawaski, K. Kallip, M. Leparoux, Graphene oxide-reinforced aluminum alloy matrix composite materials fabricated by powder metallurgy, *J. Compos. Mater.* (Submitted: 2015 16th July)

AUTHOR'S CONTRIBUTION

The present research involves the effort of numerous individuals. The reason lies in the complex nature of samples, which requires application of various experimental techniques for their characterization and an expertise of a number of scientists. The outcome produced within the framework of the research papers is a group effort. The author's contribution to each paper is given below.

I. The author was responsible for the manuscript preparation and preparation of the GO and rGO nanoplatelets dispersion using chemical and mechanochemical exfoliation techniques. The author was responsible for pretreatment of the SS and Si substrates and for deposition of GO and rGO coatings onto the substrates using the spin coating technique. The author conducted electrochemical corrosion tests and analysis. The author also participated in Raman, HR-SEM, and FTIR analyses and data plotting.

II. The author was responsible for the manuscript preparation and pretreatment of the SS substrates. The author was responsible for the PPy and GO-PPy coatings preparation using electrochemical deposition techniques. The author performed electrochemical corrosion test experiments, ASTM G48A standard test and their analyses. The author also participated in Raman, HR-SEM, FIB-SEM, and EDX analyses and data plotting.

III. The author was responsible for the manuscript preparation and preparation of the rGO nanoplatelets dispersions. The author was responsible for the SS and Si substrates preparation and rGO coating deposition on the substrates using the spin coating technique. The author also participated in ALD metal oxides (laminate) deposition process on rGO-coated substrates. The author conducted electrochemical and corrosion analysis experiments, participated in Raman, HR-SEM, FIB-SEM, and XRD measurements and in their analyses.

IV. The author was responsible for the manuscript preparation and preparation of the rGO nanoplatelets dispersions. The author was responsible for the Ti and Si substrates pretreatment and rGO coating deposition on the substrates using the spin coating technique. The author also participated in ALD metal oxides (laminate) deposition process on the rGO coated substrates. The author conducted electrochemical and corrosion analysis experiments. The author also participated in Raman, HR-SEM, FIB-SEM, and XRD measurements and in their analyses.

INTRODUCTION

This thesis studies the corrosion inhibition performance of graphene and graphene oxide based composite/hybrid coatings. Graphene is a two-dimensional one-atom-thick sheet of carbon in the form of hexagonal lattice, and it is the basic structural unit of graphite. Graphene has proven to be one of the most popular advanced materials in recent developments. Due to its many extraordinary properties, this carbon material has been widely studied for advanced applications, starting from energy harvesting and nanoelectronics and finishing with drug delivery. In this research, the atom/ion barrier property was among the most interesting ones. Some studies on using graphene or graphene-based materials as a barrier sheet had been published before this work was started, and some appeared in print during the research process. Lately, the development of graphene and graphene oxide based functionalized biocompatible barrier coatings has attracted great attention among scientists and industrialists as well. However, the use of graphene oxide/reduced graphene oxide nanoplatelets for corrosion protection of metal alloys had practically not been studied before this research, despite the fact that the idea of the preparation of these materials had been known already for decades, and relatively cheap powder of natural graphite could be used as raw material.

This thesis investigates the barrier properties of graphene/graphene oxide based nanostructured coatings, including composite and hybrid coatings, towards corrosion protection. Investigations were carried through using different strategies: for the preparation of thin protective coatings spin-coating, electrochemical deposition, and atomic layer deposition (ALD) techniques were used. For the corrosion inhibition performance studies of synthesized graphene oxide and reduced graphene oxide the hybrid coatings of graphene oxide-polypyrrole and the composite coatings of graphene-metal oxide laminates were prepared. The extent of the protection ability of the coatings deposited onto AISI type 304 stainless steel and Ti-6Al-4V alloy substrates was studied thoroughly by electrochemical methods, such as open circuit potential and Tafel plots, potentiodynamic polarization, voltammetry and electrochemical impedance spectrometry, and tested by standard ASTM G48 A and long-term immersion tests in salt solutions.

The studies revealed that prepared graphene and graphene oxide based hybrid and especially composite coatings well inhibit corrosion of the metal substrates. This definitely increases the lifetime and stability of the metal parts and equipment made from these materials, helping to preserve materials and energy, thus helping to develop a more sustainable society.

BACKGROUND

Corrosion is the deterioration of a material, usually a metal or an alloy, which results from a reaction with its environment. For example, steel rusts when immersed in seawater. The process of corrosion requires four elements: an anode, a cathode, an electrolyte, and an electrical path. Corrosion is a natural process that cannot be completely prevented, but intervention with correct measures can control it. Without intervention, corrosion progresses and becomes damaging for the corroding samples. Metals corrode because we use them in environments where they are chemically and thermodynamically unstable. Only copper and precious metals (gold, silver, platinum, etc.) are found in nature in their metallic state, all others most commonly used metals are processed from oxides or mineral ores. All these metals are thermodynamically unstable and have a tendency to revert to their more stable compound forms. Some metals form more or less protective films on their surfaces and these can almost prevent or slow down their corrosion processes depending on the environment of the sample [1]. Corrosion takes place in many different forms; the type of material, nature of the environment and length of exposure all contribute to determine the form of corrosion. Some of the most common forms of corrosions are uniform or general corrosion, pitting corrosion, galvanic corrosion, stress corrosion cracking, corrosion fatigue, crevice corrosion, and filiform corrosion [2]. The economic impact of corrosion in our society is huge. According to the World Corrosion Organization, the annual cost of corrosion in 2010 was 2.2 trillion US $, which is over 3% of world's gross domestic product (GDP; 63.0 trillion US $) [3]. Therefore, there is increased demand for robust techniques and materials that inhibit corrosion and lengthen the life cycle of products made of metal alloys, to insure great environmental and economic savings. There are several techniques reported in the literature [4–8] to preserve metallic substrates from corrosion, including surface passivation followed by painting and/or varnishing, as well as galvanic and sprayed coatings. These methods may have several imperfections such as low corrosion and mechanical resistance of passivated surfaces, low wear ability of paints, and pores and other defects in spray coatings. An alternative solution for preserving the metallic substrates is to cover their surface with a thin sealing coating, which must be dense, defect-free, and made from chemically resistive materials. The coatings should behave as diffusion barriers for environmental oxygen, water, and corrosive halide molecules/ions. Suitable methods for preparing such thin nanostructured coatings are atomic layer deposition and electrochemical deposition [9,10]. The ALD growth proceeds via cyclic deposition of sub-monolayers of a desired solid film, also allowing precise thickness control on arbitrarily shaped substrates. However, novel coatings often establish special characteristics: certain levels of hardness and elasticity, electrical and thermal conductivity, etc., which cannot be resolved using only ceramic materials. Thus, the introduction of composite nanostructure materials may be necessary. One possibility is to use carbon-ceramic coatings, which can be developed by the help of

ALD technique. Another possibility is to use carbon-polymer composite coatings on passivized surfaces, which can be developed via electrochemical polymerization from a monomer mixed with carbon material solutions-suspensions.

The use of carbon based functionalized nanostructure composite coatings to inhibit corrosion is an area getting growing attention among scientists and industrialists. Lately, graphene has started to play an important role in many applications. Graphene possesses excellent mechanical and thermal stability [11,12], low chemical reactivity [13], impermeability to most gases [14,15], and high transparency [16]. Because of these properties graphene is gaining scientists' attention in preparing protective coatings. Several groups have demonstrated the effectiveness of graphene as an oxidation resistive [17–19] and corrosion inhibitive [20–22] coating. Despite the promising properties of this new material, graphene technology still lacks methods for large-area synthesis of defect-less coatings – in [23] it was lately shown that even long period CVD synthesis of graphene on a Ni sheet at high temperature was not able to produce continuous coatings although partly the coating had already graphitic structure. On the other hand, graphite as well as defect-less graphene is on the top of the most passive materials in galvanic series, thus most metals that are covered with a graphene layer having defects will corrode very fast near the defects, which was pointed out also in [24].

This thesis has investigated the corrosion inhibition ability of mechano-chemically prepared GO and rGO nano-films followed by thin composite/hybrid coatings. We have observed a promising corrosion inhibition performance of GO and rGO films on AISI 304 stainless steel substrate [25], although modification of these materials is necessary especially when it comes to long-term inhibition. Due to the small size of the nanoplatelets, developing nonporous coatings was somewhat challenging. Therefore, our primary interest was to modify the GO and rGO materials and prepare better as well as more effective coatings.

The application of conductive polymer polypyrrole (PPy) to prepare corrosion inhibitive coatings is already known in the literature [26,27]. We developed the graphene oxide-polypyrrole (GO-PPy) hybrid coating as a modification of the GO coating. We showed that the GO-PPy hybrid coating can be used as a better replacement of GO and also as pure PPy protective coating [28]. The GO-PPy coating is dense and has low conductivity because of slight overoxidation due to GO addition to PPy. Corrosion inhibition of the substrate occurs by fending off anions through electrostatic repulsion and also by blocking the ion paths between local anodes and cathodes along the substrate-nanocomposite interface. After first successful modification, we have introduced graphene-metal oxide (rGO/Al_2O_3/TiO_2) composite coating as a modification of rGO coatings [29]. The composite coating is composed of a graphene base layer and amorphous metal oxide films as top layer. The metal oxide layer consists of aluminum dioxide (Al_2O_3) and titanium dioxide (TiO_2) nanofilms. These oxides are known for their dielectric and corrosion resistance properties [30–32].

Corrosion inhibitive performance of the advanced rGO/Al$_2$O$_3$/TiO$_2$ coating was also analyzed on AISI 304 stainless steel [33] and Titanium Ti-6Al-4V (Grade 5) alloy substrate [29]. In both cases, markedly enhanced corrosion protection performance of the composite coatings was observed. The protection ability of the GO-PPy and rGO/Al$_2$O$_3$/TiO$_2$ composite coatings was investigated through electrochemically, by standard ASTM G 48A salt test and long-term immersion in salt solutions. The analyzed results showed that these hybrid/composite coatings can be used as corrosion protective coatings, which certainly increases the lifetime and stability of the metal/alloy substrates in their long-term exploitation in corrosive environments.

GOALS OF THE RESEARCH

The main goal of this research was to investigate the corrosion protection performance of new type thin coatings, first of all graphene and graphene oxide nanofilms and their composite/hybrid coatings. The purpose of this research was to study the possibility of long-term corrosion inhibition performance by graphene (reduced graphene oxide), graphene oxide, graphene oxide-polypyrrole, and graphene-metal oxide coatings, which has not been reported in the literature. The oxidation and corrosion inhibition property of CVD grown graphene is already known. However, the barrier property of mechano-chemically produced graphene and graphene oxide nanoplatelets coatings had not been studied and reported by the time this research was conducted. This research has a task to study the above and develop better and more effective nanostructured coatings against corrosion or unwanted oxidation of the substrates, which can also be stable for a longer period of time. To fulfil this the author has to synthesize the carbon materials, to study the corrosion protection performance of mechano-chemically synthesized graphene oxide and reduced graphene oxide films, and to develop with colleagues protective graphene oxide-polypyrrole and graphene-metal oxide composite coatings for stainless steel and Ti alloy substrates. Finally, the protective performance of all the coatings has to be analyzed and tested.

EXPERIMENTAL TECHNIQUES

Preparation of graphene and graphene oxide

First, graphite oxide was prepared using modified Hummers method [29,34–37]. About 0.5 g of graphite powder (diameter <2 μm, thickness 2–6 nm, surface area of 750 m^2/g, carbon content >98 wt%, Strem Chemicals) was taken in a 500 mL conical flask. To that flask, 0.25 g of $NaNO_3$ (Sigma Aldrich) and 12 mL of H_2SO_4 (Fluka) were added and cooled in an ice bath for 30 minutes. While maintaining vigorous shaking, 1.5 g of $KMnO_4$ (Sigma Aldrich) was added slowly. The rate of addition was controlled carefully to keep the temperature of the suspension under 10ºC by using an ice bath. Then the ice bath was removed and the temperature of the suspension was brought to room temperature (22±2ºC), where it was maintained for 2−3 hours for complete oxidation of graphite powder. As the reaction proceeded, the mixture gradually thickened and became pasty, which was brownish grey in color. Then, about 25 mL of deionized water was slowly added into the paste and stirred. The suspension became brownish in color and was kept for 30 minutes. The suspension was further diluted with 50 mL warm (~60ºC) deionized water. To the diluted suspension 5 mL of 7% H_2O_2 (Fluka) was added and stirred well to completely remove permanganate ions. The resultant suspension was filtered in warm conditions and washed several times with warm deionized water. Finally, the solid brownish filtered material was re-dispersed in deionized water containing selective Ca and Na molecular sieve to remove the unwanted ions, and then filtered as well as washed several times with deionized water. Graphene oxide dispersion in water was prepared by the ultrasonication of graphite oxide (see Figure 1a). During ultrasonication, the temperature of the suspension was kept under 30ºC by sufficient cooling. The sonicated dispersion was kept for 48 hours to precipitate bigger particles out of dispersion. Then, centrifugation was performed for 8 hours at 6000 rpm, followed by decantation that was carried out by pipetting the top half of the dispersion.

(a)   (b)   (c)
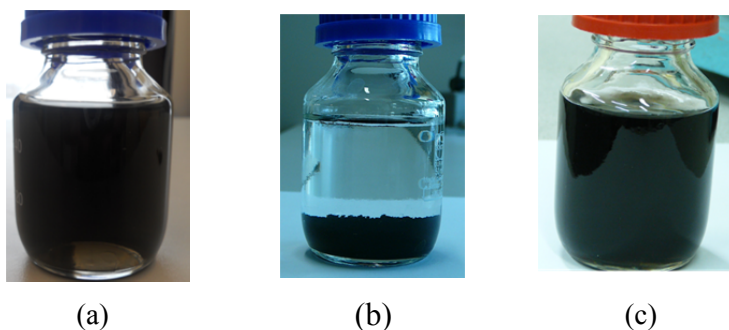
Figure 1. Images of (a) graphene oxide dispersion in water; (b) reduced graphene oxide nanoplatelets in water, and (c) the latter in organic medium N-methyl-2-pyrollidone (NMP) after 48 months of storage.

The reduced graphene oxide (Figure 1b) was prepared by the chemical reduction of GO using reducing agents (Fe/HCl) at room temperature [38,39]. In a typical experiment, 1 g of Fe powder (Sigma Aldrich) and 20 mL of HCl (37%, Fluka) were directly added into a beaker containing 100 mL of GO solution. The mixture was stirred vigorously for 6 hours to complete the reduction of GO. As reaction proceeded, the solution became black and rGO gradually precipitated out of the solution due to the hydrophobic nature of rGO platelets. After complete reduction, additional 15 mL of HCl was added into the solution in order to fully remove excess Fe powder. Finally, the resulting rGO platelets were collected by filtration and washed with deionized water and ethanol.

Substrate preparation

The substrates of AISI type 304 stainless steel were purchased from Goodfellow, UK, and Ti Grade 5 alloy was obtained from Sengewald, Germany.

The elemental composition of the alloy substrates measured by X-ray Fluorescence spectroscopy (XRF) is given in Table I.

Table I. Elemental composition of the substrate alloys.

Alloy	Element composition (mass %)							
	Fe	*Cr*	*Mn*	*Ni*	*S*	*P*	*Si*	*C*
AISI 304	70–74	18–20	≤2.0	8.0–10.5	≤0.03	≤0.05	≤1.0	<0.1
	Ti	*V*	*Al*	*Fe*	*O*	*N*	*C*	*H*
Ti6Al4V	85–90	3.5–4.5	5.5–6.7	≤0.4	<0.1	<0.1	<0.1	-

The substrates with dimensions 20×20 mm were polished and cleaned in an ultrasonic bath using toluene, followed by ethanol and isopropanol (Alfa Aesar) solvents. In each solvent the cleaning process was carried out for 10 minutes.

Coating development

The thin GO and rGO coatings on the stainless steel and titanium alloy substrates were prepared by spin coating using Spin Coater CSS-05 (PI-Kem) at 1000 rpm for 2 minutes. The 800 μL of ~0.2 mg/mL water-ethanol rGO dispersion was used to coat the substrates. The GO and rGO coatings were prepared at room temperature.

The deposition of the GO-PPy composite was carried out in a 3-electrode cell system at room temperature ($22 \pm 1^{\circ}$C), using Reference 600 Potentiostat/Galvanostat (Gamry). The GO-PPy composite was deposited on the SS

substrate that served as a working electrode (see Figure 2a). The Pt wire and a saturated calomel element (SCE) were used as counter and reference electrodes, respectively. In a typical experiment, 10 mL of aqueous GO dispersion of 0.5 mg·mL^{-1} concentration was mixed with 10 mL of aqueous pyrrole (Py) solution of 0.1 M concentration. The mixed solution was sonicated for 5 min in order to achieve homogeneous dispersion. Before the Py solution preparation, the pyrrole precursor (Fluka) was purified by distillation over calcium hydride in a laboratory vacuum-gas setup and stored in the dark, under Ar (Argon) atmosphere at a low temperature (-10°C). To the 20 mL of the previously mentioned sonicated mixed solution, 10 mL of aqueous solution of oxalic acid (Sigma Aldrich) of concentration 0.1 M (pH ≈ 1.3) was added, stirred, and poured into the above-described electrochemical cell. After that the coating deposition was started immediately. The hybrid synthesis process was carried out for ten minutes with constant current mode with a current density of 0.5 mA·cm^{-2}. The prepared coating was cleaned with deionized water and dried in air at room temperature.

(a)   (b)

(c)
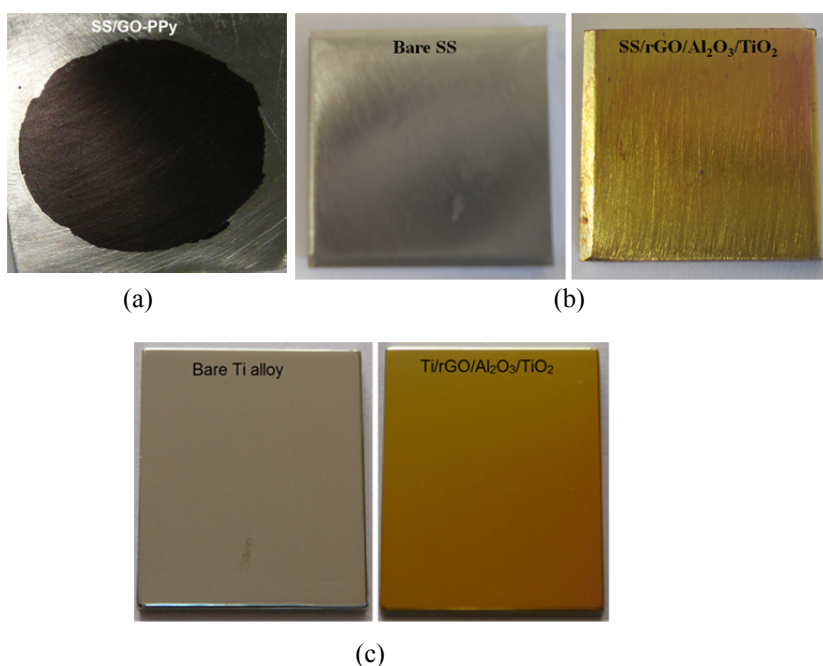
Figure 2. Bare and coated metal substrates: (a) SS substrate coated with GO-PPy hybrid coating, (b) bare and rGO/3×(Al$_2$O$_3$/TiO$_2$) coated SS substrates, and (c) bare and rGO/3×(Al$_2$O$_3$/TiO$_2$) coated Ti alloy substrates.

Thin Al_2O_3 and TiO_2 films were deposited onto the rGO coated SS (Figure 2b) and Ti alloy (Figure 2c) substrates using the atomic layer deposition technique in a flow-type low-pressure reactor [40]. For the preparation of reference samples, Al_2O_3 and TiO_2 films were deposited also on Si (1 0 0) substrates. The Si (1 0 0) substrates were cleaned by etching in HF to remove the native oxide and then rinsed in de-ionized water. In the text, the 6 films of $3\times(Al_2O_3/TiO_2)$ together, are referred to as "laminate". The Al_2O_3 and TiO_2 films were deposited in the ALD reactor under a stream of pure nitrogen gas (99,999%, AGA Estonia). The substrates were coated with 200 cycles of Al_2O_3 using the following precursors: $Al(CH_3)_3$ (TMA; 98%, Strem Chemicals) and distilled water, at the substrate temperature of 125°C, with sub-cycle periods of 3/2/2/5 s. Next, TiO_2 was deposited also for 200 cycles, using $TiCl_4$ (99.9%, Strem Chemicals) and H_2O as precursors, at the same substrate temperature and with sub-cycle periods of 2/2/2/5 s. The growth procedure was repeated for three times in order to accomplish six metal oxide layers.

Coating characterization

Both GO and rGO nanoplatelets deposited onto Si (1 0 0), SS, and Ti alloy substrates were studied with μ-Raman Spectroscope-Microscope (in Via Raman, Renishaw), with a laser beam of 514 nm. The IR radiation transmittance/absorption of the GO powder was analyzed with Fourier Transform Infrared spectroscope (FTIR; BXII, Perkin Elmer) using the potassium bromide (KBr) beam splitter and deuterated triglycine sulfate (DTGS) detector. All measurements were carried out by micro-attenuated total reflectance (μ-ATR) cell using ZnSe internal reflection element.

The surface morphology of the coated substrates was studied with high-resolution scanning electron microscope (HR-SEM; Helios NanoLab 600, FEI Company). The structural properties of the coatings were analyzed using Raman scattering and X-ray diffraction (XRD; SmartLab, Rigaku using CuKα radiation) studies. Inspection of the coatings was also made by preparing cross sections of samples with Focused Ion Beam (FIB) of the HR-SEM.

Corrosion analysis

Corrosion normally occurs at a rate determined by the equilibrium between opposing electrochemical reactions. One of them is the anodic reaction, in which a metal is oxidized, releasing electrons into the metal. The other is the cathodic reaction, in which the solution species (often O_2 or H^+) is reduced, removing electrons from the metal. When these two reactions are in equilibrium, the flow of electrons from each reaction is balanced, and no net electron flow (electrical current) occurs. The two reactions can take place on one metal or on two dissimilar metals (or metal sites) that are electrically connected. Figure 3 sketches this process. The vertical axis indicates the electrical potential

and the horizontal axis shows in logarithmic scale the absolute value of total current density. The theoretical current for the anodic and cathodic reactions is represented as straight lines. The curved line is the total current: the sum of the anodic and cathodic currents. The sharp point in the curve is actually the point where the current reverses polarity as the reaction changes from anodic to cathodic, or vice versa. The sharp point is caused by plotting along the logarithmic axis. The use of the logarithmic axis is necessary because of the wide range of current values that must be recorded during a corrosion experiment. Because of the phenomenon of passivity, the current often changes by six orders of magnitude during a corrosion experiment.

The potential of the metal is the means by which the anodic and cathodic reactions are kept in balance. Figure 3 shows that the current component of each half reaction depends on the electrochemical potential of the metal. Let us suppose that the anodic reaction releases too many electrons into the metal. Excess electrons shift the potential of the metal to more negative, which slows the anodic reaction and speeds up the cathodic reaction. This counteracts the initial perturbation of the system. The equilibrium potential assumed by the metal in the absence of electrical connections to the metal is called the corrosion potential, E_{corr}. The value of either the anodic or cathodic current at E_{corr} is called the corrosion current density, I_{corr}. If we could measure I_{corr}, we could use it to calculate the corrosion rate of the metal. The above description of the corrosion process does not say anything about the state of the metal surface. In practice, many metals form an oxide layer on their surface as they corrode. If the oxide layer inhibits further corrosion, the metal is said to be passivated (as in this study), in this case I_{corr} is represented as I_{pass}, passive current density. In some cases, local areas of the passive film break down, allowing significant metal corrosion to occur in a small area. The potential in which passive film breakdown occurs is called pitting potential, represented as E_{pit}. This phenomenon is called pitting corrosion or simply pitting.
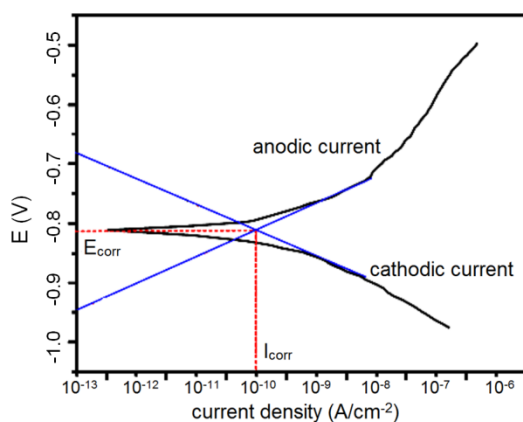
Figure 3. Corrosion process showing the anodic and cathodic components of the total current.

The corrosion inhibition ability of the substrates was assessed by monitoring the open circuit potential (E_{ocp}), potentiodynamic polarization, voltammetry, Tafel plot, electrochemical impedance spectrometry (EIS), and a test of a long-term immersion in salt solution. The electrochemical measurements were carried out at room temperature, in 3.5 % NaCl aqueous solution for AISI 304 stainless steel, and in 1 M aqueous KBr solution for Ti-6Al-4V titanium alloy. The standard ASTM G48A salt test analysis (a test for pitting and crevice corrosion resistance of stainless steel alloys) was carried out to study SS/GO-PPy coating durability. The samples were immersed into 6 % ferric chloride ($FeCl_3 \cdot 6H_2O$; Sigma Aldrich) aqueous solution, the pH of which was adjusted to 1 by adding HCl acid. The test was carried out for six days. The tested substrates were examined with a high-resolution scanning electron microscope. A minimum of two samples were tested per condition, in order to guarantee reproducibility. The E_{ocp} was measured under continuous immersion after the potential stabilization. Potentiodynamic polarization was carried out in a potential range, from -250 to +250 mV, with a standard scan rate of 0.125 mV/s. Reference 600 Potentiostat/Galvanostat (Gamry Instruments) was used for all the electrochemical measurements. A PTC1^{TM} test cell (Gamry) was used to fix the samples as working electrodes and contain the solution, while Port Holes^{TM} Masks (Gamry) were used to limit the exposed area of the sample to 1 cm^2. A three-electrode arrangement had the potassium chloride saturated calomel electrode (SCE; Evikon MCI OÜ) as reference and a platinum wire as counter electrode.

Electrochemical impedance spectrometry (EIS) was carried through in a frequency range from 0.01 to 10^5 Hz, with nine points per decade, with a sinusoidal excitation potential of 10 mV (amplitude RMS) applied around the E_{OCP}, and measured after the stabilization of the latter, i.e. under steady state conditions. Fitting of the spectra was done using Zview® 2.70 software (Scribner Associates, NC, USA), in which depressed capacitive loops are treated as constant phase elements (CPE) [41], whose impedance is given by Z_{CPE} [42]:

$$Z_{CPE} = \frac{1}{(j\omega)^n Q} \tag{1}$$

In this approach it is assumed that the micro-roughness and heterogeneity of the surface generates a non-uniform distribution of charge, which results in a dispersion of the time constants ($\tau = RC$, where R is resistance and C is capacitance) responding at different frequencies. With this interpretation, Q is the frequency-independent component and is proportional to the area of the active sites that contribute to the process, whereas the exponent n indicates the deviation from an ideal dielectric behavior, being $n = 1$ for an ideal capacitor and $n = 0$ for an ideal resistor [42].

A minimum of two samples were analyzed per condition to guarantee reproducibility.

GRAPHENE AND GRAPHENE OXIDE BASED PROTECTION AND FUNCTIONALIZATION OF STAINLESS STEEL SURFACE

(Paper I)

Characterization of nanographene and its coating

The GO prepared using modified Hummers' method is dispersed in water and in organic solvents (ethanol and N-methyl-2-pyrrolidone). Due to the presence of a large variety of oxygen functional groups in the GO structure, the material becomes polar and hydrophilic in nature, which enhances the dispersibility of GO [35].

(a)

(b)

(c)

(d)
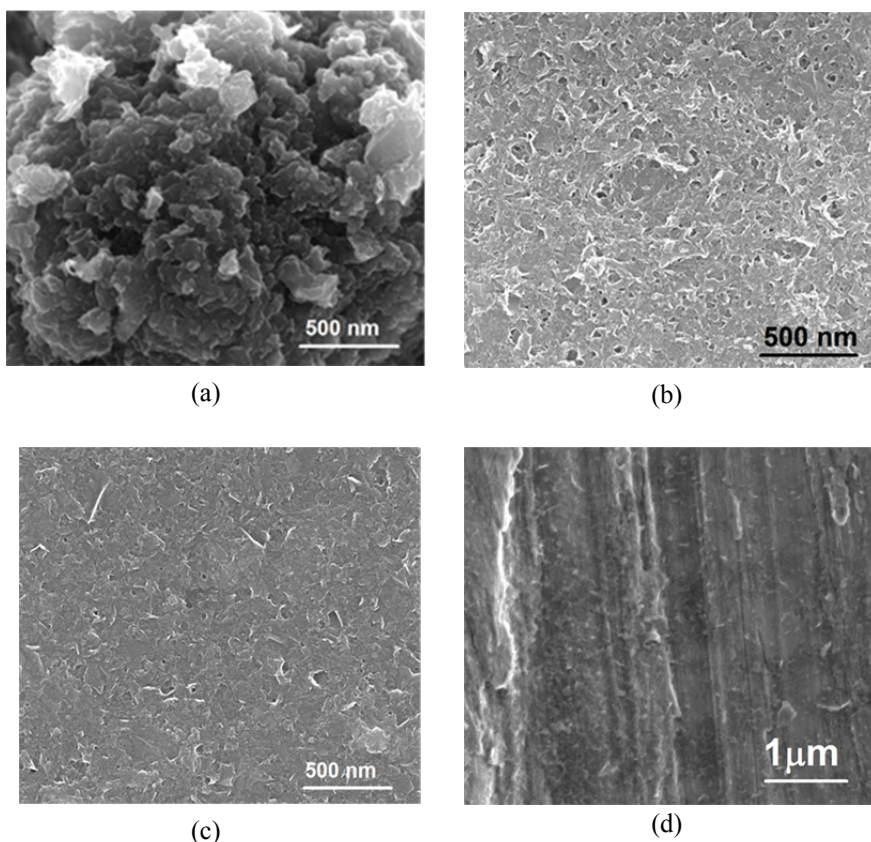
Figure 4. HR-SEM images of: (a) graphite powder (row material), (b) GO film on Si (1 0 0), (c) GO coated SS, and (d) rGO coated SS substrates.

Figure 4 shows HR-SEM images of GO and rGO coated surface morphology on Si (100) and SS substrates. Dimensions of rGO nanoplatelets become smaller than GO nanoplatelets; this could be the effect of an additional reduction process, which generates additional defects that are also showing more intense D band in the Raman spectrum than the ones for GO (see Figure 5), and more defective nanoplatelets can be destroyed more easily during the sonication process. Raman spectra of raw graphite powder, GO and rGO nanoplatelets deposited on Si substrates were also studied (Figure 5). The carbon material generally shows characteristic G and D bands.
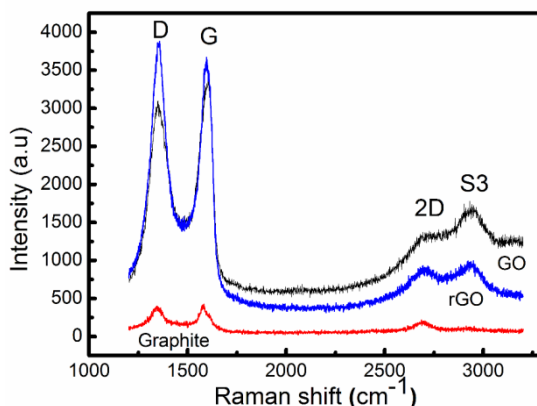

Figure 5. Raman spectra of graphite powder (raw material), and synthesized GO and rGO films on Si (1 0 0) substrate.

The G band at ~1582 cm^{-1} arises from first order scattering of phonon E_2g symmetry at the Γ point of the first Brillouin zone of graphite and involves in-plane bond stretching of sp^2 carbon pairs [43,44], whereas the D band at 1350 cm^{-1} arises from the breathing mode of K (kappa) point phonons of A_1g symmetry. The D band appears only in disordered carbon materials and its intensity is connected to the presence of six-fold aromatic rings [39,45]. High values for the ratio of the integrated intensities of the D and G bands (I_D/I_G) are usually taken as an indication of disorder in the structures. The I_D/I_G ratio values for graphite powder and GO nanoplatelets were 0.97 and 0.90, respectively. After chemical reduction, the I_D/I_G ratio was increased to 1.18, suggesting an increase of the disorder level of the material. A similar increase of the ratio I_D/I_G has been reported in the literature [46–50]. Alternatively, this increase could result from the smaller lateral scale of graphene flakes, which would increase the concentration of defects [38, 39]. However, it has also been suggested that GO is an amorphous state and that the graphitic state can only recover after reduction, which means that the I_D/I_G ratio cannot be directly compared between these two states [45,51]. The presence of a large number of hydroxyl, carboxyl and

other oxygen consisting groups in the GO structure decreases the relative number of aromatic rings, diminishing the intensity of the 2D band [47]. Such decrease in aromaticity agrees well with the low electrical conductivity of GO. After chemical reduction, most of the oxygenated functional groups were removed, increasing both the aromaticity and the electrical conductivity in the rGO structure. This reduction process could be limited if the aromatic areas in rGO are small and thus the relative intensity of the D band is in sum increasing, leading to the increase of I_D/I_G ratio. The S3 band observed at 2882 cm^{-1} resulted in a combination of phonons connected with the D and G bands.

The extent of the reduction of the GO material was also analyzed by FTIR spectroscopy. The IR transmittance spectrum of GO (Figure 6) showed two strong absorption peaks at 3422 and 1117 cm^{-1}. The first one was caused by the stretching vibration of both structural OH groups and adsorbed water molecules; the second one was due to typical C─O structural vibration. The C─H, O=C─H, C=O, and C=C stretching vibrations were also found, at 2924, 1706, 1567, and 1382 cm^{-1}, respectively [52, 53]. After chemical reduction, the assigned high intensity peaks were diminished. The band corresponding to OH groups, which appeared at 3427 cm^{-1}, was also observed for the KBr matrix. The band at 1633 cm^{-1} can be assigned to stretching of the adsorbed water molecules [54–56]. During the reduction step, the carboxyl groups present in the GO structure cannot be easily reduced [57]. These groups could remain untouched during the reduction process and are most probably localized at the edges of graphene nanosheets.
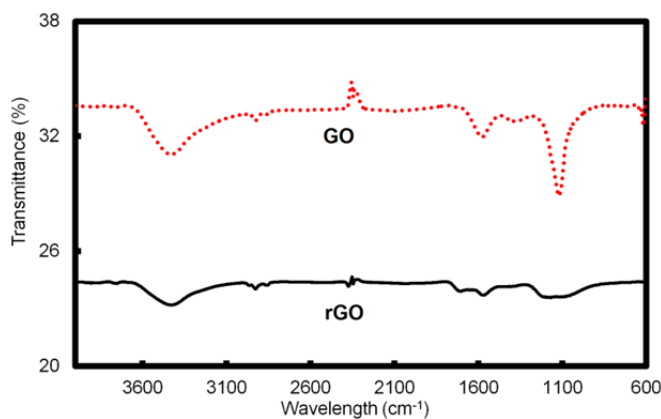

Figure 6. FTIR spectrum of GO and rGO nanoplatelets measured in KBr matrix.

Their presence should not deleteriously influence the electronic properties of graphene nanoplatelets. The spectra also contain a component from the skeletal vibration of un-oxidized graphitic domains [56, 57].

Protection performance of the
GO/rGO coatings on SS substrates

Figure 7 represents the results of open circuit potential change of the GO and rGO coated and bare SS substrates measured in aqueous NaCl solution. The potential shifted towards anodic direction when GO and rGO covered the substrate surface, indicating that the surfaces were affected by electrochemical processes. The GO and rGO coated samples showed relatively stable potential values as compared to the bare substrate. However, all of the samples showed transients towards a negative potential. The transients were smallest for the GO coated substrate.
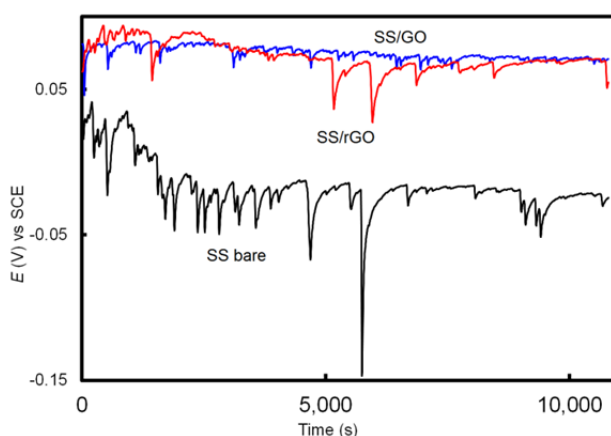
Figure 7. Open circuit potential of the SS bare, SS/GO and SS/rGO-coated SS samples for 3 h stabilization in 3.5 % aqueous NaCl solution.

These transients indicate meta-stable pit formation on the sample surface that was briefly passivated. The coatings with fewer transients reflect better passivity against localized corrosion. As is seen in Figure 7, the sample with GO coated surface showed the best E_{OCP} stability, but the rGO coating also inhibited the potential stability after 1.5 h. This result primarily indicates the passivity of GO and rGO coatings. Furthermore, to analyze the extent of passivity, we performed a potentiodynamic polarization analysis before and after 30 days' immersion of the coated samples in the salt solution. The corrosion potential, passive current density, and pitting potential were determined from potentiodynamic plots shown in Figure 8. The E_{corr} of the bare, GO and rGO coated substrates was found to be –10, +44 and +20 mV, and the I_{pass} 54.2, 28.1 and 26.2 nA/cm^2, respectively. The shift of E_{corr} to a more anodic region and the decrease of I_{pass} reflect the formation of a passive layer on the alloy surface that works as a passive barrier against the penetration of corrosive Cl$^-$ ions, thus providing protection against corrosion.
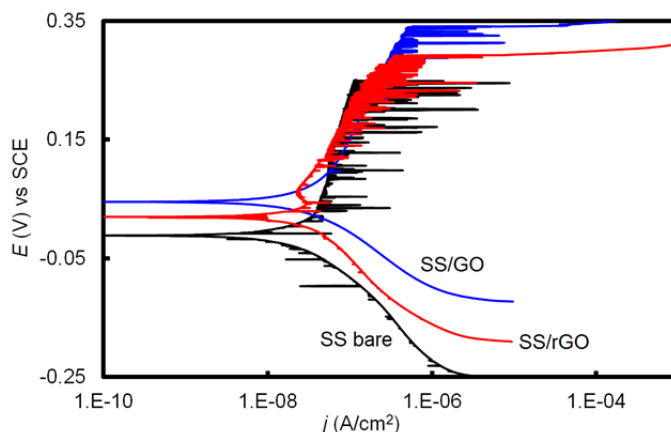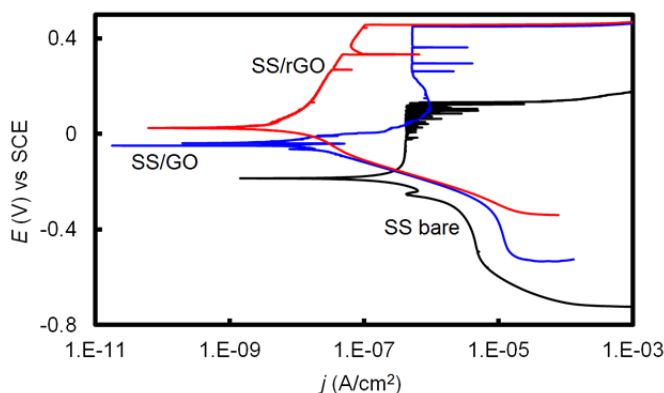
Figure 8. Potentiodynamic plot of SS bare, SS/GO and SS/rGO coated samples measured in 3.5 % aqueous NaCl solution.

The E_{pit} for the bare, GO, and rGO coated samples was found to be 236, 340, and 284 mV, respectively. The above data analysis suggests that the GO coated sample exhibited a better protection ability than the rGO coated one, revealing a better passivity of the GO nanoplatelets as we already showed in the E_{OCP} analysis above. This is probably due to the presence of a wide range of oxygen containing functional groups in the GO structure, which may give a negative charge density to the coating [58]. For that reason, the coating creates an electrostatic repulsion against corrosive Cl^- ions. Moreover, both GO and rGO coatings minimized the formation of meta-stable pits in the cathodic potentials of the polarization curves. Nevertheless, the coatings failed to block the formation of meta-stable pits in the anodic potential part, although the rate of the meta-stable pits formation was reduced to some extent in comparison to the curve belonging to bare SS substrate. In polarization plot (Figure 9) samples after thirty days immersion in the salt solution showed that the E_{pit} of the GO and rGO coated substrates increased to +451 and +457 mV, respectively. These results imply that even after long immersion time the GO and rGO coated samples showed much higher passivity than the bare substrate.

The results indicate that nanographene passive layers remain quite stable in the salt solution for a long time. Surprisingly, the tests shows that the rGO coated sample seems to be even a little more passive at the end of the long-term test than the GO coated one. However, it is interesting that the formation of meta-stable pits on the GO and rGO coated samples is reduced to a significant extent (compare plots in Fig. 8 and 9).

Figure 9. Potentiodynamic plot of the bare SS, SS/GO and SS/rGO coated samples after 30 days immersion in 3.5 % aqueous NaCl solution.

Figure 10 shows HR-SEM images of the surface morphology of bare, SS/GO, and SS/rGO coated samples after a month of the immersion test, where the formation of corrosive products is barely noticeable, especially on the SS/GO surface, which directly indicates the barrier property of the nanographene coatings. It is highly probable that even after long immersion the GO and rGO coatings can still protect, to some extent, the formed passive layer from the corrosion attack. However, to increase the adhesion of substrate-nanoplatelets and maximize the protection efficiency, modifications are needed. As an advanced modification of the GO and rGO coatings, we have developed a GO-polymer (GO-PPy) hybrid coating, which enhances the protection performance and substrate stability for a longer period of time.

(a)

(b)

(c)
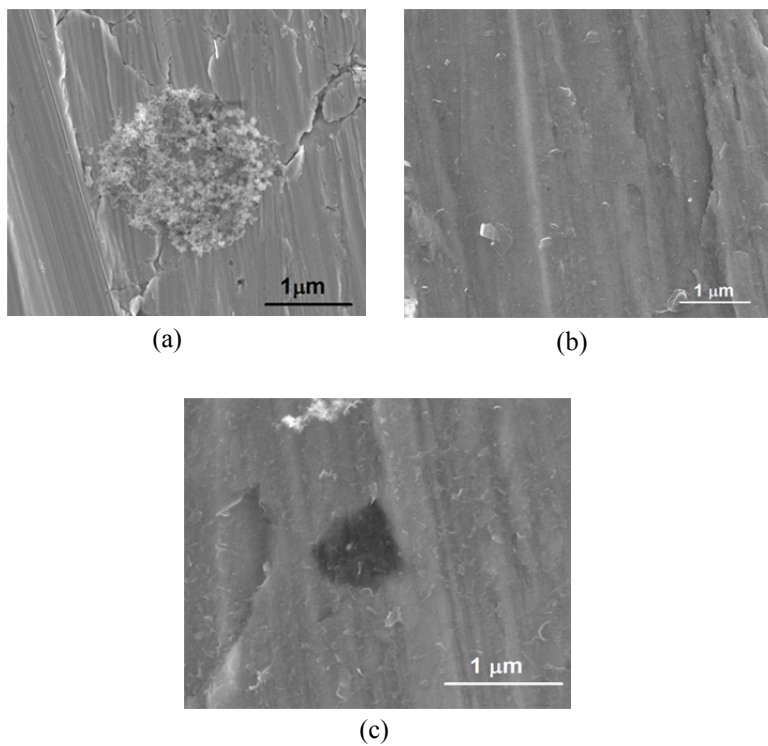
Figure 10. HR-SEM images of (a) bare SS, (b) SS/GO, and (c) SS/rGO coated samples after thirty days immersion in 3.5 % aqueous NaCl solution.

PROTECTION AND FUNCTIONALIZATION OF SS SURFACE BY GO-PPy COMPOSITE/HYBRID COATING

(Paper II)

## Coating morphology and structural properties

As a modification and functionalization of GO coatings we deposited a GO-polypyrrole (GO-PPy) composite/hybrid coating onto the SS substrate. The electrochemical GO-PPy composite deposition mechanism was compared with the polypyrrole (PPy) deposition mechanism. During galvanostatic electrodeposition, the depositional potentials for both were recorded and the results are presented in Figure 11. At the beginning of the PPy deposition, the potential increased rapidly to 0.72 mV, which is the peak potential, then rapidly dropped down to 0.68 mV, followed by re-increase to 0.73 mV, which is the polymerization potential. During GO-PPy deposition, the potential of the system was slightly decreased and then reached the polymerization potential, at 0.69 mV. This lower polymerization potential for the GO-PPy composite material compared with the PPy is likely due to the presence of the negative charge on the GO sheets and indicates the involvement of GO nanosheets in the polymerization (oxidation) reaction as "doping anions", as mentioned also in earlier works [59, 60].
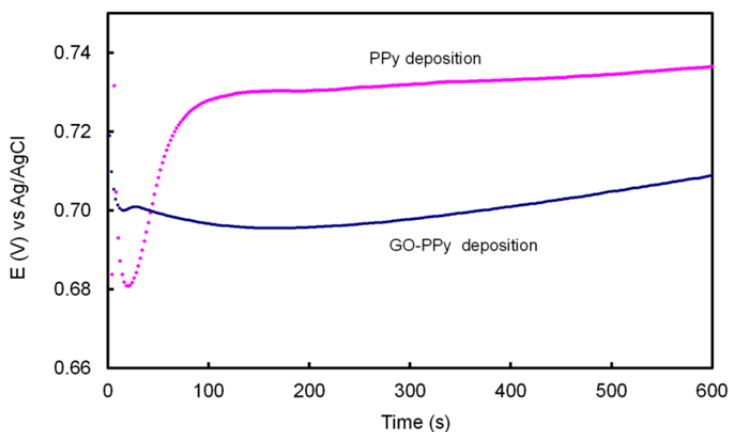
Figure 11. Potential change during galvanostatic synthesis of PPy and GO-PPy in aqueous solution of oxalic acid during depositing the coatings onto SS substrates.

It is expected that during ultra-sonication, the positively charged Py cation radicals could first attach at the basal planes and edges of a negatively charged GO surface, and then the polymerization of Py would occur on the surface of the

GO sheet. There is strong π-π stacking interaction between the GO sheet and the electronic structures of the conjugated backbones of PPy. Thus, a compact GO-PPy composite is synthesized and it is well bonded to the alloy substrate, to which the relatively rough surface of the SS substrate also makes a contribution.

(a) (b)
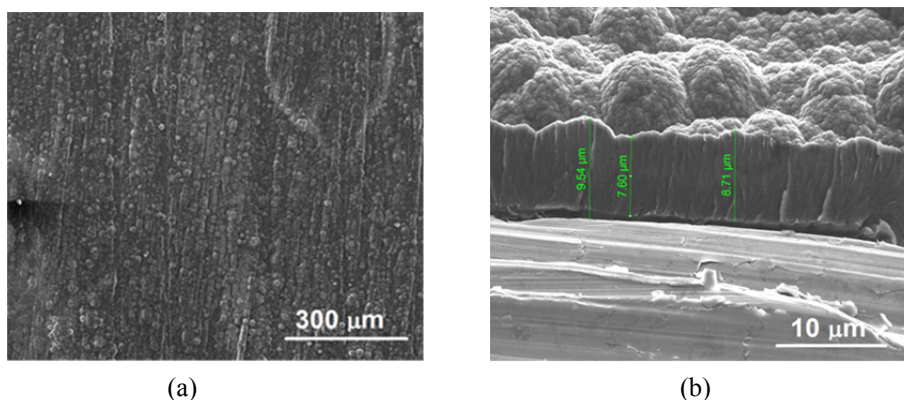
Figure 12. HR-SEM images of: (a) surface of GO-PPy coating deposited on SS substrate, and (b) the coating cross-section with the marks of coating thickness measurement.

Figure 12 shows the surface morphology of the GO-PPy composite coating on the SS substrate. The coating morphology is homogeneous, has well-known cauliflower structure, is dense without visible pores, and covers the substrate even better than the previously studied GO film (see Figure 3c). The coating thickness obtained was ~ 9 μm (Figure 12b).
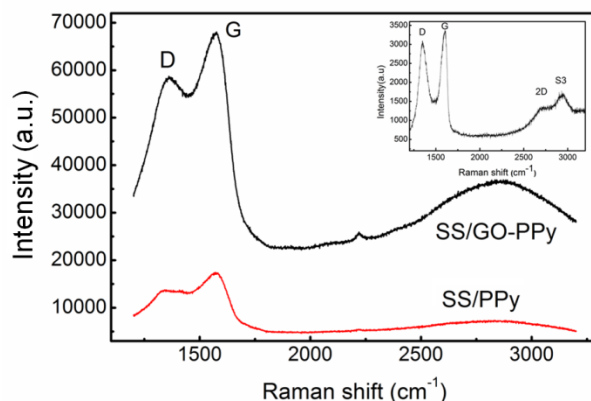
Figure 13. Raman spectrum of PPy, GO-PPy and GO (inset) coated SS substrate.

28

In Figure 13, the Raman spectra of the PPy and GO are compared with the GO-PPy nanocomposite. One can see that the spectrum of PPy is characterized by two broad bands near 1355 and 1582 cm^{-1}, respectively. These two bands correspond to the ring stretching of the polymer backbone and the π-conjugated structure [61,62]. In the spectrum of the GO-PPy composite, the D and G bands of GO nanoplatelets are not clearly visible due to overlapping with the high intensity broad bands of PPy in the same area.

Protection performance of the GO-PPy coating on SS substrates
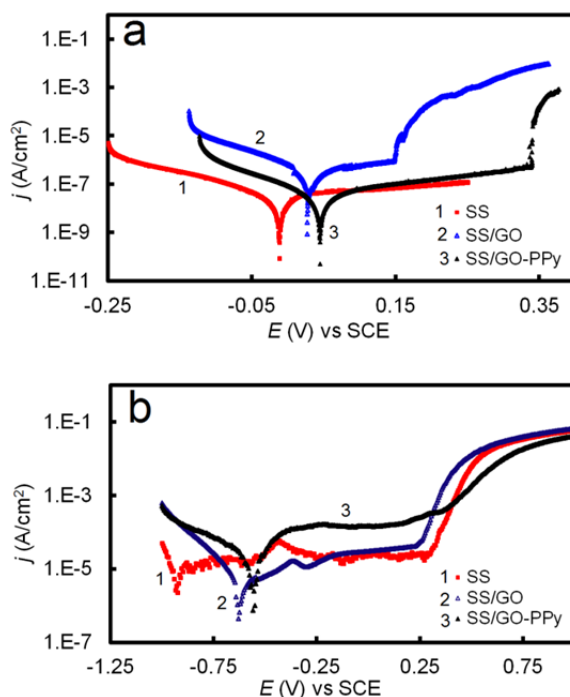
Figure 14. Electrochemical analysis of bare and coated SS samples measured in 3.5 % NaCl aqueous solution: a) Tafel plots, and b) voltammetry plots.

The extent of corrosion protection by this composite coating was obtained from Tafel and voltammetry analysis. E_{corr}, I_{corr}, and E_{pit} values were obtained from Tafel plots as given in Figure 14a, and from voltammetry plots as given in Figure 14b. The E_{corr} for the GO-PPy composite coating had a value of 48 mV; for the GO and uncoated surface it was observed at 32 and -9 mV, respectively. The value of I_{corr} for the composite coating was determined to be 6.0 nA, which is much lower than that of bare and GO coated substrates. The E_{pit} for the uncoated, GO, and GO-PPy coated samples was observed at 243, 300, and 360

mV, respectively. These analyzed experimental findings reflect the best passivity of the composite coating. To justify this result, voltammetry scan was also performed (see Figure 14b). The E_{corr} and E_{pit} values showed a trend similar to that in Tafel analysis for all the samples. However, a higher anodic current density value was noticed for the GO-PPy coated sample. This could be because of the higher scan rate (10 mV/s) that was applied. Because of this higher scan rate, the system could not get enough time to stabilize itself.

Furthermore, the stability of the GO-PPy composite coating was investigated in a highly corrosive environment. The standard ASTM G48A ferric chloride pitting test was analyzed for six days, and the resultant substrates were examined with an HR-SEM.
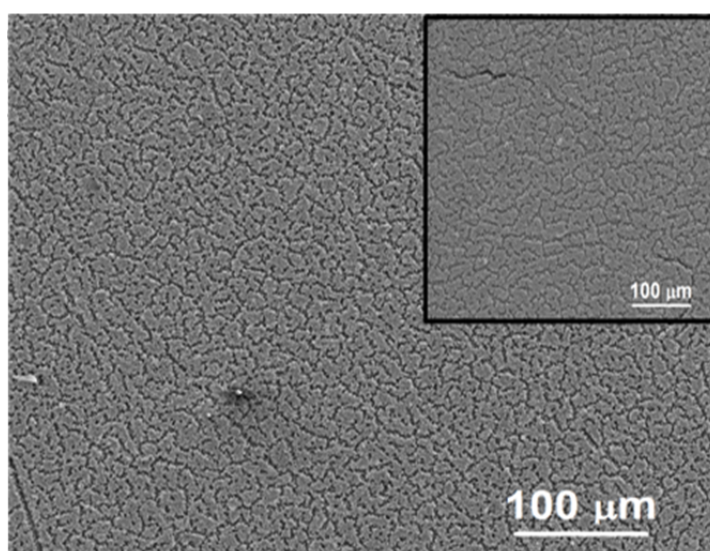
Figure 15. HR-SEM image of graphene oxide-polypyrrole composite coated stainless steel substrate after 72 h and after 144 h (inset) immersion according to the ASTM G48A standard immersion test.

Figure 15 presents HR-SEM images of the composite coating after 72 h and 144 h (inset) of immersion in aggressive ferric chloride aqueous solution. The coating was noticed to be stable more than 72 h (which is the standard testing time). After 144 h of immersion, the coating structure deteriorated and coating breakdown was noticed in some areas. The positive effect of the addition of GO nanoplatelets in the GO-PPy composite was clearly observed in the increase of the coating resistance. However, the resistance efficiency of the coating can probably be further increased, yet more research and experimentation is needed.

DEVELOPMENT OF CERAMIC-GRAPHENE NANOLAMINATE COATINGS FOR CORROSION PROTECTION OF STAINLESS STEEL

(Paper III)

Coating morphology and structural properties

The rGO coated substrate (Figure 16a) reveals a rough surface that cannot be distinguished from the bare substrate (not presented), due to the transparency of the nanoplatelets to the electron beam under working conditions. The application of the laminate ($3 \times (Al_2O_3/TiO_2)$) resulted in a smoother surface, although the polishing marks could still be detected on the deposit (Figure 16b). The morphology changed when the substrate was first coated with rGO nanoplatelets, resulting in a globular morphology of the composite deposit (Figure 16c). However, the cross section of the rGO/laminate substrate could not be adequately resolved by the HR-SEM to avoid microscopic damage because of the magnetic substrate (Figure 16d). A similar coating system was applied on the silicon substrate to better understand the coating formation and coating structure, which revealed a striped structure of six alternate alumina and titania layers of relatively uniform and compact materials and with a total thickness of ~150 nm (inset in Figure 16d).
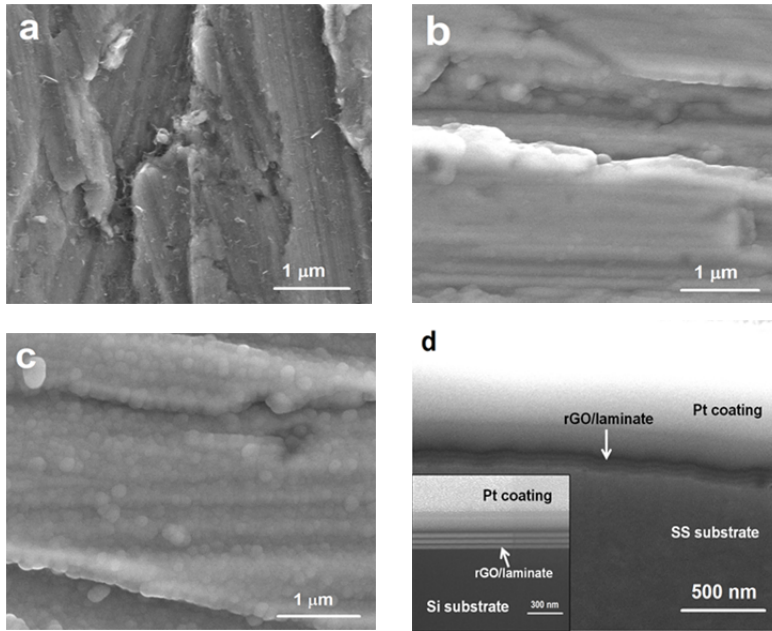
Figure 36. HR-SEM micrographs of a) SS/rGO, b) SS/laminate, c) SS/rGO/laminate, and d) cross-sections of the SS/rGO/laminate and Si/rGO/laminate substrate, in the inset.

The peak intensity ratio of D and G bands (I_D/I_G) in the Raman spectra of the rGO coated substrate before and after lamination was found to be 0.96 and 0.98, respectively (Figure 17). The G band position for the same was measured at 1595 and 1592 cm^{-1}, respectively. These changes indicated that oxygen in the Al_2O_3 film was not chemically bonded to rGO nanoplatelets. For chemically bonded oxide, the I_D/I_G ratio should have increased and the G band position should have downshifted significantly [63, 64]. The low intensity and wide bands found at 179, 447, and 608 cm^{-1} (spectra 2 and 3) indicated an amorphous structure of the oxide films, which was expected because they were grown at a relatively low temperature (125ºC) [65, 66], whereas the sample with layered oxide only had no indication of crystalline carbon.
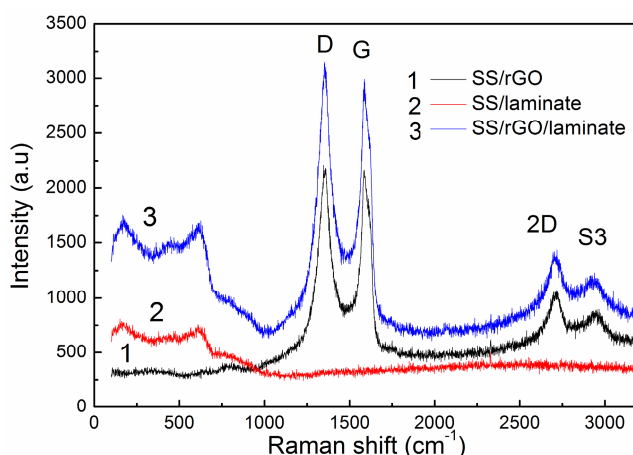
Figure 17. Micro-Raman spectra of the SS/rGO (curve 1), SS/laminate (curve 2) and SS/rGO/laminate (curve 3) samples.

When deposited onto the rGO coating, the Al_2O_3/TiO_2 layer provides good coverage of the surface; this is not usually observed with the CVD grown or micromechanically extracted graphene [67], and suggests that some water mol-ecules or OH^- groups have been physisorbed onto the surface of the rGO nano-platelets. It has been reported that graphene can physisorb small molecules such as H_2O, NH_3, O_3, and NO_2 [68–71], which may work as active sites for the ad-sorption of the aluminum precursor, favoring nucleation and growth of the Al_2O_3. These molecules can become adsorbed on graphene due to a partial charge transfer from graphene to N/O atoms. The irregular structure including the borders/sides of the rGO nanoplatelets further enhances the adhesion of the metal oxide films via the ALD technique. The growth of the TiO_2 film on the Al_2O_3 layer is easier because the alumina acts as an "adhesion layer." However, the direct growth of the TiO_2 film on the graphene surface is hindered because the basal plane of graphene is unreactive [72, 73].

Protection performance of the ceramic-graphene nanolaminate coatings on SS substrates

Figure 18 demonstrates the results of a long-term (30 days) immersion in neutral 3.5% NaCl solution of the laminate only (Figure 18a) and rGO/laminate (Figure 18b) coatings. The first coating was seriously damaged during the test: it was broken and delaminated. The image reveals a large corrosion pit generated by more passive phase particles, seen on the pit bottom. The second coating is without any visible defects and has even preserved the fine structure of the laminate surface seen magnified in the inset – the surface structure is very similar to that in Figure 16c, imaging the surface of an as-grown rGO/laminate. Thus, the corrosion inhibition property of the laminate significantly improved upon introduction of an interface layer of the rGO nanoplatelets. This observation primarily indicates the application of graphene-metal oxide nanocomposite to protect the SS substrate from corrosion.
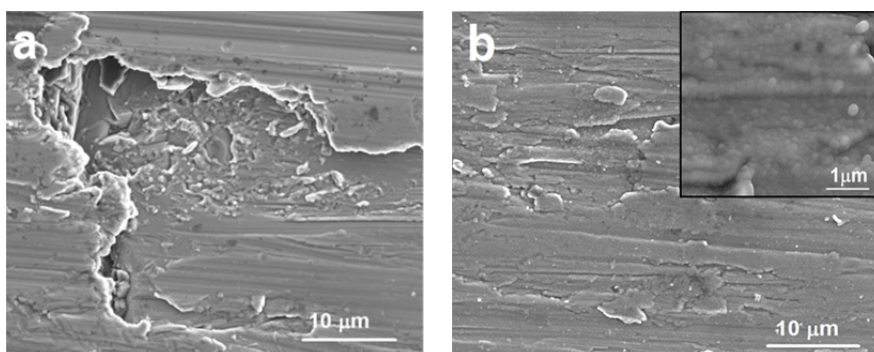
Figure 18. HR-SEM micrograph of the samples of a) SS/laminate, and b) SS/rGO/laminate after 30 days of immersion in neutral pH 3.5 mass% NaCl aqueous solution at room temperature; the inset in part *b* shows the surface structure in more detail.

Further investigations were made by means of electrochemical analysis. Under passive conditions and at neutral pH, the cathodic reaction on the surface is the reduction of oxygen, reaction formula (2), while the anodic reaction is the passive dissolution of the alloy, reaction formula (3), namely at weak points like pores in the coated samples.

$$O_2 + 4e^- + 2H_2O \rightarrow 4OH^- \quad\quad\quad (2)$$
$$Fe^0 \rightarrow Fe^{2+} + 2\ e^- \quad\quad\quad (3)$$
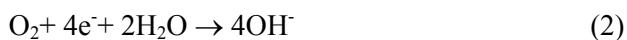
The bare alloy presents reasonably stable open circuit potential values, in the range of 0 to +0.20 V. These values are typical of passive stainless steel and

indicate residual dissolution under anodic kinetic control. A few anodic transients indicate metastable pits, i.e., instantaneous breakdown of the passive film at weak spots, followed by reconstruction of the film (Figure 19).

The open circuit potential was shifted toward the less noble potentials when the laminate layers covered the surface (curves SS/laminate and SS/rGO/laminate), which may have resulted from anodic depolarization, i.e., increase of the residual passive dissolution due to the increased surface area or increased surface conductivity, or from cathodic polarization, i.e., to a hindered cathodic reaction. All samples showed a relatively stable potential, although with anodic transients. These transients were relatively small in the bare sample but quite significant in the samples covered with only rGO or only laminate. In contrast, the SS/rGO/laminate substrate was quite stable, with hardly any transients, thus indicating a more stable passive film.
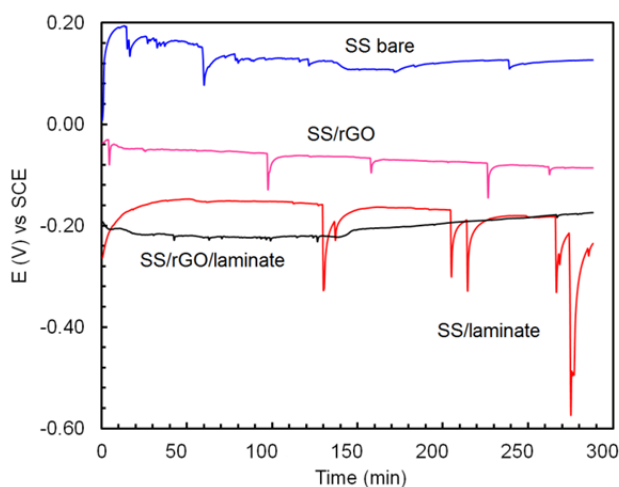
Figure 19. Open circuit potential of the coated systems measured in neutral pH 3.5 mass% NaCl aqueous solution, for bare alloy (SS bare), alloy coated with an rGO thin film (SS/rGO), alloy with a laminate oxide coating (SS/laminate), and a composite hybrid coating (SS/rGO/laminate).

The corrosion potential extracted from the polarization plots supports the observations of the spontaneous potential in Figure 19. Potentiodynamic polarization reveals passive behavior in all the samples. Compared to the bare sample, the rGO surface has a marginally wider passive plateau because the pitting potential has shifted only by ~5 mV in the anodic direction (Figure 20). However, numerous metastable pits are observed in both samples; these events become more frequent as the potential becomes more anodic, and are commonly associated with weak points in the top layers. The application of the laminate onto the bare alloy causes a drop of the passive current by approximately three orders of

magnitude. The laminate by itself does not totally eliminate the formation of metastable pits, whereas the SS/rGO/laminate sample clearly exhibits the best passivity with the lowest passive current, the highest pitting potential, and hardly any current transients. The potential and current transients observed in the potential measurements (Figure 19) and in the polarization plots (Figure 20) reveal the formation of metastable pits (i.e., fast nucleation of local anodes that re-passivate after a few seconds) [74]. These events occur at a spontaneous potential but become more frequent and more intense under increasing anodic polarization. They can be observed on all samples with the exception of the full system (i.e., the rGO/laminate), which reveals not only compatibility but also synergy between the two layers. These pits eventually lead to active corrosion whenever one of those pits does not re-passivate and therefore the synergistic effect of the graphene-ceramic composite coating is significantly beneficial in terms of corrosion protection. The graphene seems to work against the generation of local electric fields in the substrate near-surface area: first, acting as a diffusion barrier for corroding ions, and second, increasing the conductivity of the interface (otherwise formed by natural oxides of the substrate), thus screening local electric fields. To be sure that the deposition of the alumina ALD film onto the rGO film does not decrease the electrical conductivity of the latter, the film conductivity was measured before and after the deposition of a monolayer of alumina. It produced the anticipated result that the electrical conductivity of the rGO film increases considerably, approximately two times, probably due to further reduction of rGO by TMA during the first cycles of ALD. Thus, the possibility of the rGO interface layer to screen the local electric fields is even improving after the laminate deposition. On the other side, it seems that the interface layer preserves a certain electrochemical activity, so that it is not generating quick galvanic corrosion even by scratching the coating, as was shown in the preliminary tests.
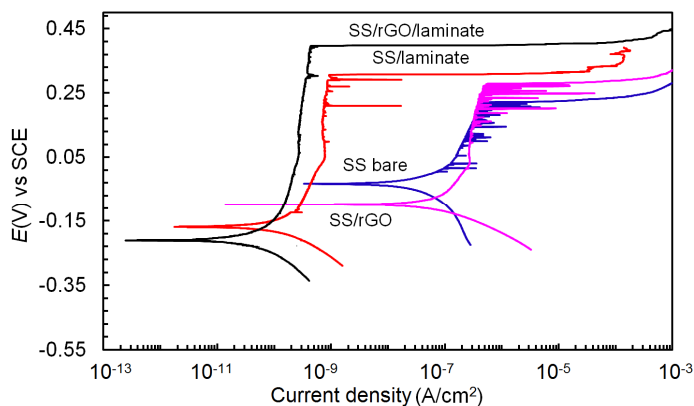

Figure 20. Potentiodynamic polarization plots of the SS samples with different coatings measured in neutral pH 3.5 mass% NaCl aqueous solution at room temperature.

The EIS analysis yielded good reproducibility and the representative spectra are presented as both Bode and Nyquist representations (Figure 21). The |Z| Bode plot presents a straight line with a slope of -0.5 (Figure 21a), which corresponds to a capacitor. This capacitive behavior goes down to the low frequency end of the spectrum, which indicates that the charge transfer has very low kinetics. The ohmic resistance is measured at high frequencies only in bare and rGO coated samples but not in the samples with laminate due to the low capacitance of the coatings, which causes a shift in the spectrum towards higher impedance, moving the ohmic resistance out of the frequency window. The laminate applied directly onto the steel produces two capacitive regions separated by a resistive plateau at intermediate frequencies, in which the high frequency capacitance can be assigned to the alumina/titania film, and the low frequency portion of the spectrum is nearly coincident with the spectrum of bare steel, thus corresponding either to the fraction of the steel surface that was not covered or to the pores of the laminate film. Because the HR-SEM and TEM analyses provided no proof of non-coated areas and porosity of as-grown by ALD amorphous oxide laminates, the pores or cracks could be generated into the coating during the open circuit potential stabilization in the electrolyte before the electrochemical measurements or during the measurements. The resistive plateau in the Bode curve can be associated with the resistance of the electrolyte inside the channels or cracks in the laminate [75, 76].

The full rGO/laminate system gave the highest impedance value, followed by the metal oxide (laminate only) and the bare substrate, whereas the role of the rGO layer by itself was only minor. Native oxides on stainless steels were expected, and the corresponding capacitance and resistance were $\sim 10^{-5}$ μF cm^{-2} and $\sim 10^{6}$ Ω cm^{2}, respectively, in agreement with the typical values found in the literature [77, 78]. Fitting an equivalent circuit (EC) with a single time constant was attempted for the bare substrate (Figure 22a). In this circuit, R_s is the solution resistance, R_{SS} is the resistance of the native oxide, and Q_{SS} and n are the constant phase element parameters attributed to the dielectric behavior of the native oxide film (see equation 1 in paragraph 2 and fitted parameters in Table II). This EC accurately describes the high frequency portion of the spectrum, above 0.1 Hz, where the passive film is measured (Figure 21a, b).

The EIS spectrum for the rGO-coated substrate shows a single capacitive loop in the Nyquist plot (Figure 22c). However, the fitting made using the EC in Figure 22b with two time constants, corresponding to the rGO layer response at high frequencies and to the native oxide response at low frequencies, was found to be adequate (Figure 21d). In this situation, the capacitance of the native oxide and that of the rGO layer are of the same order of magnitude. The resistance of the rGO layer is low (Table II) and of the same order of magnitude as that of the solution, which indicates contact between the electrolyte and the underlying layer of the native oxide [78].
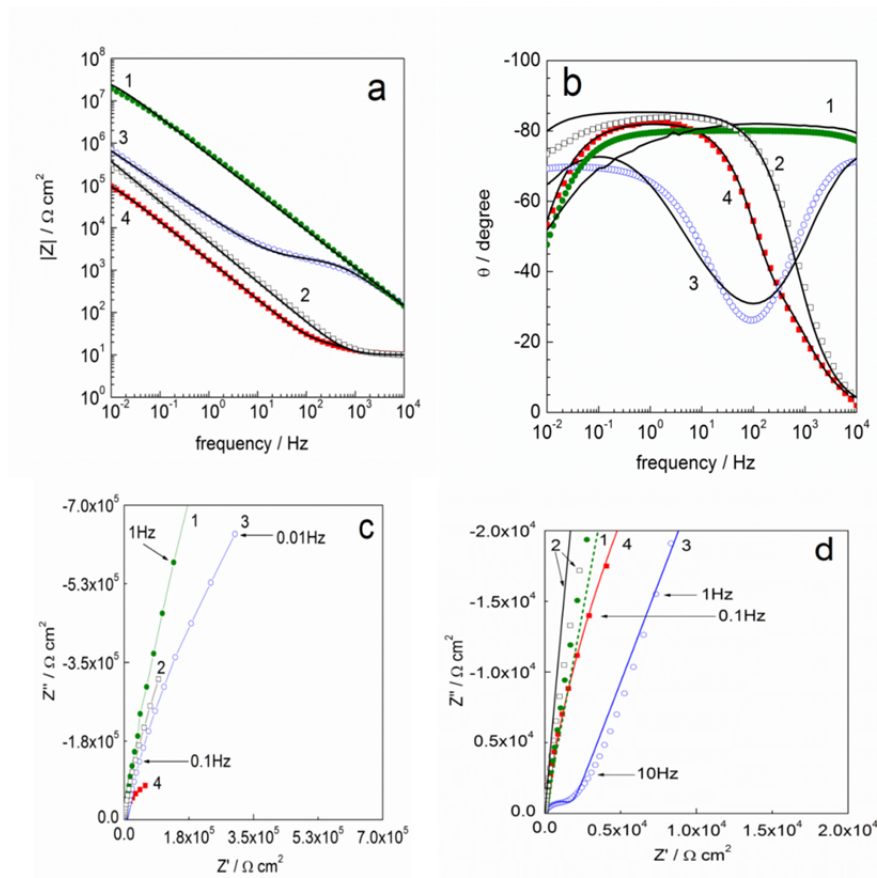
Figure 21. Electrochemical impedance spectra measured at steady state in neutral pH 3.5 mass% NaCl aqueous solution at room temperature: a) Bode plots in impedance amplitude presentation with experimental points and with fitting lines, b) Bode plots in phase angle presentation with experimental points and with fitting lines, c) Nyquist plots with experimental points connected with lines, and d) Nyquist plots with experimental points and with fitting lines. The line numbers (symbols) are used to indicate data for: SS/rGO/laminate 1 (full rings), bare SS 2 (open squares), SS/laminate 3 (open rings), and SS/rGO 4 (full squares).
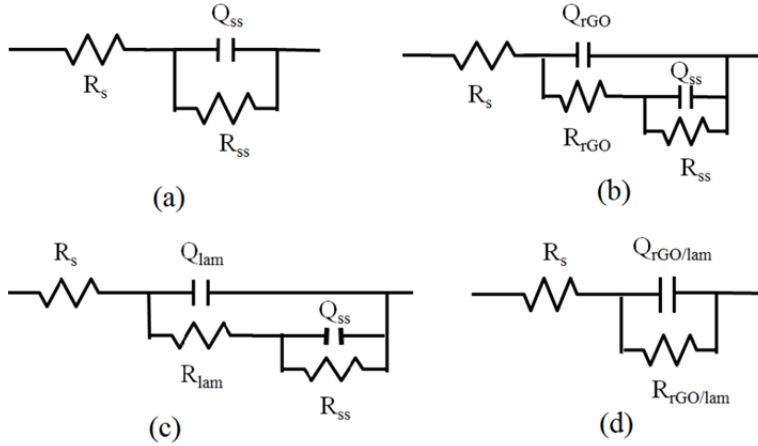
Figure22. Electrical equivalent circuits used to fit EIS data for a) bare SS, b) SS/rGO, c) SS/laminate, and d) SS/rGO/laminate substrates. The subscripts indicate the solution (S), substrate (SS), metal oxide laminate (lam), and full system, which is graphene metal oxide laminate (rGO/lam).

The capacitance can be calculated from the standard equation:

$$C = \varepsilon_0 \varepsilon \, A/d \tag{4}$$

where ε is relative dielectric constant, ε_0 is the permittivity of vacuum (8.85×10^{-14} F/cm), d is the thickness of the rGO layer (2–3 nm), and A is the surface area (1.0 cm^2). Considering a capacitance of ~76 µF, the resulting dielectric constant for the rGO layer should be ~203, which is in good agreement with the literature [79, 80].

Compared to the passive alloy, the laminate layer is thicker and thus a lower capacitance should result according to Equation 4. The process in the high-frequency region can be represented by six RC circuits placed in a series, corresponding to the layered alumina and titania films, which would theoretically result in a capacitance of 1.65×10^{-7} F cm^{-2}, considering the thickness of each metal oxide layer to be $d(\text{Al}_2\text{O}_3) = 42$ nm, and $d(\text{TiO}_2) = 15$ nm, and the dielectric constants for the TiO$_2$ and Al$_2$O$_3$ oxides as 30 [81] and 8 [82], respectively. It is interesting that the capacitance is constant at high frequencies, while the corresponding resistance varies (Table II); this is related to the fact that the indicators measured are the resistance of the native oxide in the case of the bare substrate and the resistance of the electrolyte through the pores of the coating in the laminate system.

Table II. EIS Fitting Parameters.

System	R_{ss}, Ω cm^2	Q_{ss}, Fcm^{-2}s^{n-1}	n	R_{rGO}, Ωcm^2	Q_{rGO}, Fcm^{-2}s^{n-1}	n	R_{lam}, Ωcm^2	Q_{lam}, Fcm^{-2}s^{n-1}	n	χ^2
Bare SS	3.8×10^6	3.7×10^{-5}	0.92	-	-	-	-	-	-	0.0033
SS/rGO	2.0×10^5	3.3×10^{-5}	0.98	28.0	7.6×10^{-5}	0.89	-	-	-	0.0012
SS/ laminate	3.6×10^7	1.3×10^{-5}	0.78	-	-	-	1.9×10^3	5.0×10^{-7}	0.87	0.0108
SS/rGO/ laminate	4.0×10^7	-	-	-	-	-	-	3.7×10^{-7}	0.89	0.0463

A single time constant was found to be sufficient to describe the full system (SS/rGO/laminate) accurately (see the EC in Figure 22d and the fitting results in Figure 21d). The coating reveals a high coverage of the surface and so only the electrochemical response of the ceramic layer is measured. The theoretical and experimental values of the laminate capacitance agree, indicating that the rGO layer has little influence on the dielectric properties of the coating but does help preserve its corrosion protection properties.

Porosity Evaluation

Since the electrochemical results suggest a porous structure for the laminate, the sealing performances of the laminate and rGO/laminate coatings were estimated in the surface fraction of the substrate exposed to the electrolyte. Defects in the coating were assumed to connect the bulk electrolyte to the substrate surface where the corrosion reactions occurred. Several electrochemical methods have been proposed to evaluate the coating porosity [83–87]. For smooth films, the porosity (P) can be estimated from the passive current density extracted from the polarization curve at a potential of +0.2V anodic with respect to the open circuit potential, for the coated sample i_p and for the bare sample i_p^0 [87,88]:

$$P = \frac{i_p}{i_p^0} \times 100 \ (\%).
\tag{5}$$

The passive current densities and the estimated porosity are shown in Table III. The rGO coated steel is very rough and therefore the method cannot be applied. The laminate layers show very low porosity and the full system can be considered to form a good physical barrier, which is in agreement with its electrochemical response in chloride medium.

Table III. Passive Current (i_p) Density and Coating Porosity.

System/Parameters*	i_p^0 ** (A/cm^2)	i_p** (A/cm^2)	P*** (%)
SS/laminate	3.5×10^{-6}	5.0×10^{-10}	1.4×10^{-2}
SS/rGO/laminate		2.0×10^{-10}	5.7×10^{-3}

* All parameters determined for the samples immersed into neutral pH 3.5 mass% NaCl aqueous solution at room temperature;

** i_p^0- and i_p- passive current densities estimated from potentiodynamic data of bare SS and coated SS samples, respectively, at potentials $E = E_{COR} + 0.2$ V, where E_{COR} is corrosion potential;

*** P- porosity, estimated by Equation 5.

PROTECTION AND FUNCTIOLIZATION OF Ti ALLOY WITH GRAPHENE NANOPLATELETS-METAL OXIDE COMPOSITE COATINGS

(Paper IV)

Coating morphology and structural properties

Similar rGO-metal oxide coatings are also applied on Ti Grade 5 alloy substrate. When the Al_2O_3 (alumina) and TiO_2 (titania) metal oxide nanocoating (laminate) is applied directly on alloy substrates, these metal oxides take a round shape, which seems to follow the rough morphology of the substrate (Figure 23a). When the same metal oxides are applied onto the rGO layer, the morphology of the metal oxides is quite different (Figure 23b).

(a)   (b)
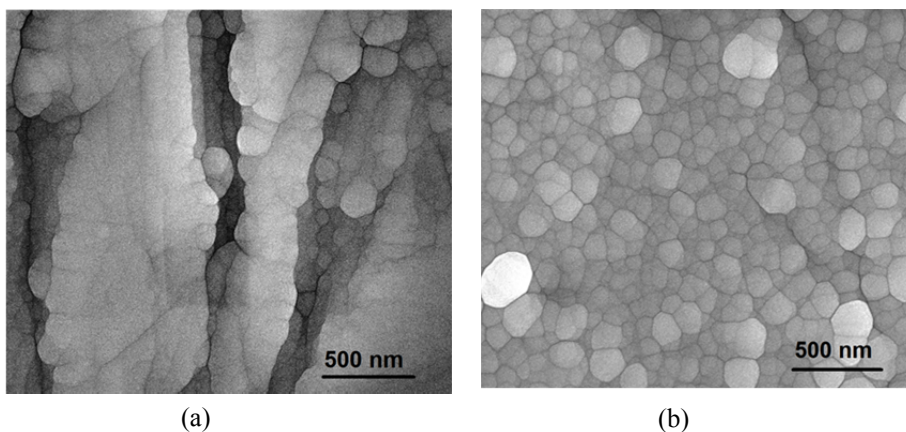
Figure 23. HR-SEM images of: (a) Ti-alloy/laminate and (b) Ti-alloy/rGO/laminate surfaces before testing.

The surface has a well-defined globular structure, with small grains of approximately 0.1 μm; this structure is typical of amorphous metal oxides. The nucleation of metal oxides on the rGO surface is clearly good as the metal oxides cover the surface homogeneously. The rGO/laminate coatings have been developed on Ti alloy substrates. The cross section of the Ti-alloy/rGO/laminate sample (Figure 24) shows a very thin dark layer of rGO nanoplatelets covered by a striped structure that corresponds to the six sublayers of metal oxides laminate, finally covered with Pt protective coating deposited locally with the FIB (topmost).
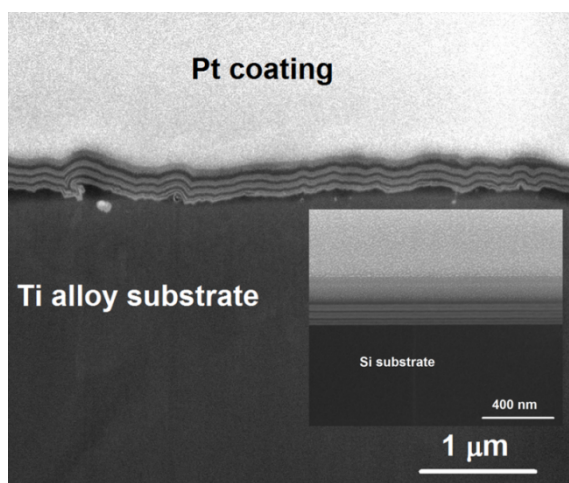
Figure 24. FIB-SEM cross section image of rGO/laminate coated Ti-alloy and Si substrate (inset).

The coating has a total thickness of ~200 nm and it is compact. A similar coating has also been prepared on Si substrate as reference and is shown in the inset (Figure 24). The Al_2O_3 sublayer, deposited directly onto the rGO surface, well covers the graphene layer, which is not common for CVD or micromechanically extracted natural graphene. The growth of the TiO_2 film becomes easier when it applies onto the Al_2O_3 layer. The alumina film thus acts as an "adhesion layer", enabling an easier growth of the TiO_2 film than that on the graphene surface directly. This effect we saw already during deposition of similar coatings onto SS-substrates in paragraph 7, and it is discussed there in more detail.
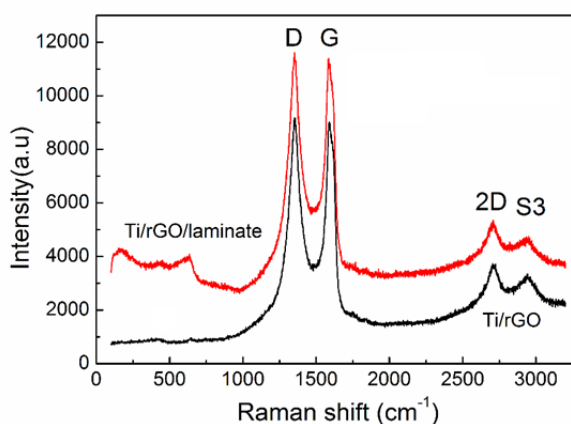

Figure25. Raman spectrum of rGO and rGO/laminate coated Ti-alloy substrate (Ti).

The Raman spectrum of rGO, laminate, and rGO/laminate coatings is shown in Figure 25. Commonly a change in I_D/I_G ratio as well as a shift of the G band after ALD lamination provides information about the nature and structure of the metal oxide films on the graphene surface. The I_D/I_G ratio before and after lamination was found to be 0.95 and 0.97, respectively.

The G band positions for the above were measured at 1595 and 1592 cm^{-1}, respectively. These changes indicate that the oxygen from the Al_2O_3 film is probably not chemically bonded to rGO nanoplatelets. If they had been chemically bonded, the I_D/I_G ratio should have increased significantly and the G band position would have downshifted to a greater extent. Some low intensity bands at 170, 438, and 613 cm^{-1} were also observed and revealed the amorphous structure of the oxide films, as expected for films grown at relatively low temperatures.

The X-ray diffraction (XRD) patterns for both laminated substrates, with and without the rGO film (Figure 26), confirm that the deposited oxides are amorphous. In fact, the introduction of the rGO layer affected somewhat the relative intensity of the main diffraction peaks, but the diffraction peaks measured are the same and correspond to the spectrum of titanium alloy.
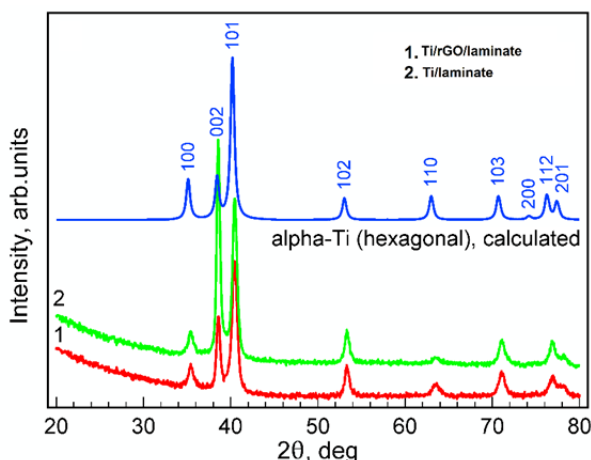
Figure 46. X-ray diffraction pattern of Ti-alloy/rGO/laminate (curve 1) and Ti-alloy/laminate (curve 2) samples, and theoretical curve of pure hexagonal Ti (top curve).

Protection performance of graphene-metal oxide (rGO/laminate) composite coatings on Ti alloy substrate

After successful evaluation, the rGO-metal oxide coating is applied on the Ti alloy substrate. The corrosion inhibition of titanium and its alloys in chloride medium is recognized as remarkably good. The naturally formed passive oxide layer on it is quite stable against moist chloride, ClO_2^-, hypochlorous acid, and salts like $NaCl$, KCl, NH_4Cl, $MgCl_2$, $BaCl_2$, $CuCl_2$, and $FeCl_3$ neutral solutions

[89]. However, passive metals and alloys can be prone to pitting corrosion under aggressive conditions, particularly in the presence of halide salts. Among halide salts, bromides seem to be the most aggressive to titanium alloys [2]. For that reason, the corrosion inhibition ability of the prepared coatings was studied in aqueous potassium bromide solution. As a primary analysis, the surface microstructures of the substrates were studied upon long-term (40 days) immersion test in the salt solution. The rGO/laminated substrate remained unaffected: no visible coating delamination or coating breakdown was noticed (Figure 27c), whereas the other substrates were severely affected by corrosive bromide anions (Figure 27a, b). The salt test analysis primarily demonstrated that the rGO-metal oxide coating can be used as an effective corrosion inhibitor.

(a)   (b)

(c)
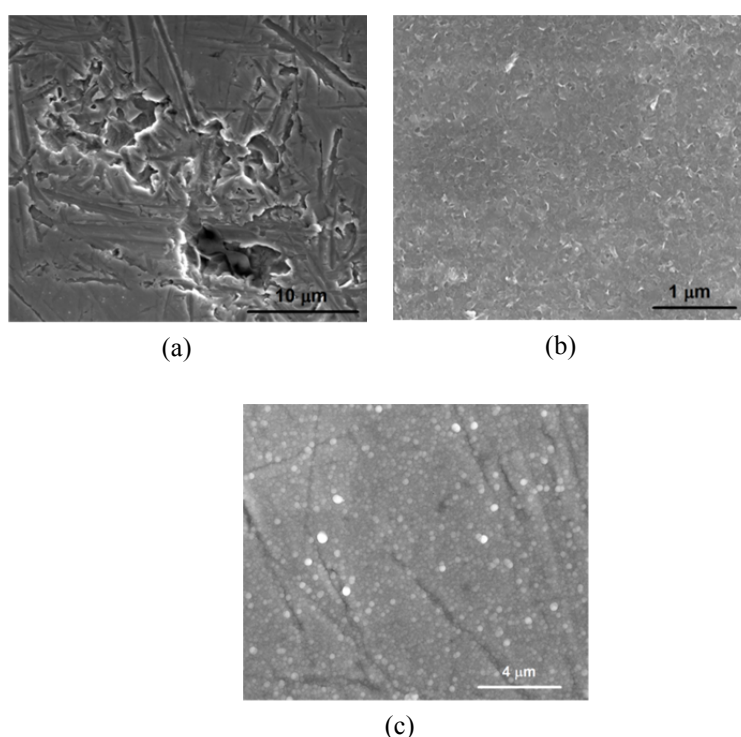
Figure 27. HR-SEM images of: (a) bare, (b) coated with rGO, and (c) coated with rGO/laminate Ti-alloy substrates after 40 days exposure in 1 M KBr aqueous solution.

The above analysis was further confirmed through electrochemical tests. The polarization test of the substrates was carried out in continuous immersion for 2 hours, see the open circuit potential curves in Figure 28. The potential was quite stable in all the samples within the duration of the experiment, which is normal for passive systems and reveals stable systems, with no signs of pitting corrosion. According to the Pourbaix diagrams, the OCP of all the systems was in the

region of passivity [2]. Still, the laminate caused a shift to more active potentials, probably due to the presence of aluminum oxide.
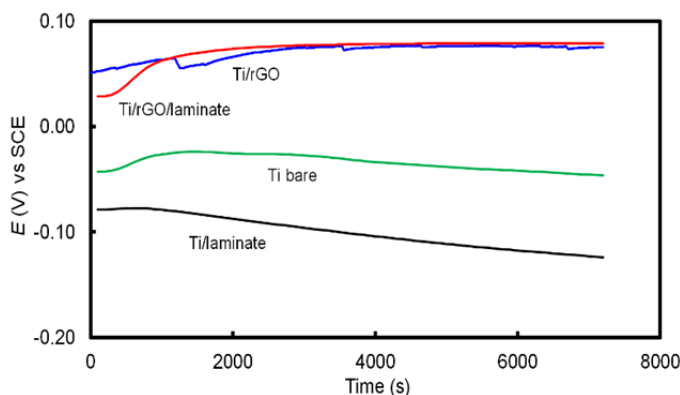
Figure 28. Open circuit potential (Eocp) of bare and coated Ti-alloy substrates (Ti) measured in 1 M KBr aqueous solution.

The systems with the rGO layer (both with and without the laminate) had a shift of ~100 mV in the anodic direction. The polarization plots given in Figure 29 were obtained starting from a cathodic potential. The corrosion potentials obtained from the curves were all shifted in the cathodic direction as compared to the E_{OCP} values, due to the changes induced by the cathodic part of the experiment on the surface and also in the local pH. The potential shifts were all around -200 mV, whereas the sample with the laminate had a shift of -400 mV only, which indicates that it was more susceptible to the cathodic polarization, i.e., it was more reactive.
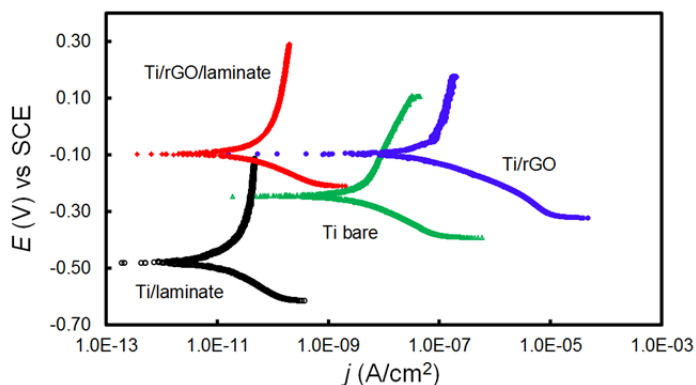
Figure 29. Tafel plots of the bare, rGO-, laminate-, and rGO/laminate coated Ti-alloy substrates (Ti) measured in 1 M KBr aqueous solution.

From the potentiodynamic plots, open circuit potential, passive current density, and pitting potential vales for all the samples were determined and is presented in Table IV.

Table IV. Open circuit potential (E_{OCP}), passive current density (I_{pass}), and pitting potential (E_{pit}) values.

Sample	E_{OCP} (mV, SCE)	I_{pass} (nA/cm^2)	E_{pit} (V v. SCE)
Ti bare	-40	2.2	1.1
Ti/rGO	70	140	0.4
Ti/laminate	-120	0.03	3.0
Ti/rGO/laminate	80	0.1	5.5

The rGO film increases the passive current, possibly due to increased surface conductivity or active area, whereas the samples with the laminate (both with and without the rGO underneath) have the lowest passive current dissolution. The slope of the cathodic branch of the polarization plots is the same in all cases, indicating that the reduction reaction is probably the same, which at this pH should be the reduction of dissolved oxygen. The pitting potential was determined from the fast anodic polarization curves shown in Figure 30. The value of E_{pitt} of the bare and rGO coated substrates was found to be 1.1 and 0.4 V, respectively. The E_{pit} for the only laminated and rGO/laminated substrates was found to be as high as 3.0 and 5.5 V, respectively. The above analysis suggests that the rGO/laminate coating exhibits a much better inhibition ability than others by increasing the E_{OCP} and lowering I_{pass} value. The inhibition ability is thus significantly increased upon introducing the rGO nanoplatelets film between the metallic substrate and metal oxide layers. The above experimental analysis demonstrates that the rGO/metal oxide laminate coating can act as a good corrosion inhibitor. This composite material can be used to prepare better and effective protective coatings for the Ti-alloy substrate, which definitely increase the lifetime of the substrates.
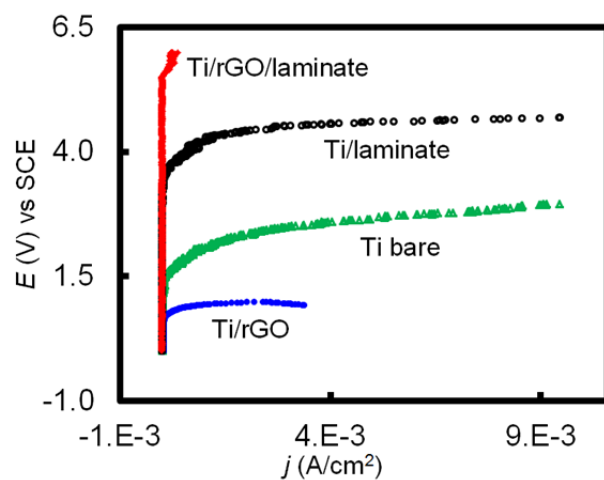
Figure 30. Voltammetry plots of the bare, rGO coated, Al_2O_3/TiO_2 laminated, and rGO/Al_2O_3/TiO_2 laminated Ti-5 substrates measured in 1 M KBr aqueous solution.

CONCLUSIONS

In this study the preparation technology of GO and rGO nanomaterials and of their simple coatings, GO-PPy hybrid and rGO/3×(Al$_2$O$_3$/TiO$_2$) composite coatings was elaborated and described, the coatings' properties were investigated, and their performance to act as thin corrosion protective coatings was tested. The study was carried through in a complex way, using different thin film preparation techniques: spin-coating, electrochemical deposition, and atomic layer deposition, and a number of solid sample characterizations and testing methods available at both the Institute of Physics and the Institute of Chemistry of the University of Tartu were used.

The extent of corrosion protective performance of the coatings before and after long-term immersion in salt solution was investigated through the measurement and determination of the open circuit potential, Tafel plots, voltammetry curves, electrochemical impedance, as well as by carrying through standard ASTM G48A salt test and long-time immersion in aqueous sodium chloride or potassium bromide solution, depending on the coating material and the substrate used.

The main results and novelty of the studies presented in the thesis are as follows:

- ✓ Preparation of graphene oxide and reduced graphene oxide nanoplatelets, both as dispersions in water/polarized organic solvents and powders, using as raw material powder of natural graphite, and a modified mechanochemical method was introduced and exploited;

- ✓ Preparation technologies of thin GO and rGO simple coatings, GO-PPy hybrid and rGO/n×(Al$_2$O$_3$/TiO$_2$) composite coatings were elaborated and exploited for coating AISI type 304 stainless steel and Ti-6Al-4V titanium alloy substrates. Spin coating was used for the preparation of the simple graphene based coatings, electrochemical deposition for the hybrid coating, and atomic layer deposition technique for the composite coating;

- ✓ The simple thin coatings of GO and rGO nanoplatelets exhibited a limited protection of the metallic substrates and can find usage in mild corrosive environments or for relatively short-term using. Nevertheless, the coatings cannot protect the SS samples against the pitting corrosion in neutral salt solutions for a longer period;

- ✓ The hybrid GO-PPy coating on the SS substrate, with a thickness of ~ 10 µm, was the thickest one that was studied in this work, and it showed medium protection of the substrate, well withstanding a 72 h ASTM G48A standard immersion test. But after 144 h testing time cracks and openings were seen in the coating, which means that it had lost its protective character. For that reason, this type of coating could be used in medium corrosive environments and probably also in medicine for coating some implants and prostheses: the PPy is known as a biocompatible material, and the coating preparation technology allows to easily add into

it drugs or anti-inflammatory impurities for better treatment of the patients during and after surgery. Unfortunately, this coating cannot be used on the surfaces exposed to hard mechanical contacts and/or wearing because of the low hardness and wearability of the material;

✓ The composite coating consisting of the rGO underlayer and the metal oxide laminate ($3\times(Al_2O_3/TiO_2)$) top layer prepared by the ALD method showed good corrosion inhibition properties, which were demonstrated by both the electrochemical measurements (increased pitting potential, decreased corrosion and passivation currents, and lowered coating porosity) and the successful long-term salt solution immersion tests. It is important to point out that the laminate or the graphene layers alone could not protect the metal substrates against pitting corrosion; the possible reasons are given and discussed in the thesis;

✓ Finally, three types of corrosion coatings developed and tested in this thesis showed different levels of corrosion inhibition and can be used in different applications. This allows us to declare that the application of the study results increases the lifetime and stability of metal parts and equipment made from these materials, helping to save materials and energy, and thus to develop a more sustainable society.

SUMMARY IN ESTONIAN

Uudsed nanostrukuursed korrosioonivastased komposiitkatted

Antud doktoritöös uuriti grafeenoksiidi (GO) ja redutseeritud grafeenoksiidi (rGO, edaspidi grafeen) valmistamise tehnoloogiat ja kirjeldati seda, valmistati nende ainete baasil lihtkatted, hübriidkatted koos polüpürrooliga (GO-PPy) ja komposiitkatted koos metalloksiidide kiledega (rGO/(3×(Al$_2$O$_3$/TiO$_2$)), edaspidi laminaat), mis kanti roostevaba terase (AISI 304, lüh. SS) või Ti-sulamist (Ti-6Al-4V, lüh. Ti5) valmistatud aluste pindadele. Katted valmistati vurr-katmisega (GO ja rGO katted), elektrokeemilise sadestamisega (hübriidkatted) ja kombineeritud vurr- ning aatomkihtsadestamisega (komposiitkatted). Uuriti antud katete omadusi, kasutades laia hulka tahkisobjektide karakteriseerimise vahendeid, mis on saadaval TÜ Füüsika ja Keemia instituutides ning määrati nende katete võimet pidurdada alusmaterjalide korrosiooni korrodeerivates soolalahustes. Viimastes katsetes kasutati nii pikaajalisi immersiooniteste, näiteks standardne ASTM G48A soolatest või immersioon NaCl (või KBr) vesilahustes kui ka suhteliselt kiireid elektrokeemilisi mõõtmisi-analüüse, näiteks avatud vooluahela pinge üleskirjutus, Tafeli ja voltamperomeetriliste kõverate mõõtmine, elektrokeemilise impedantsi spektromeetria ja modelleeriv analüüs.

Antud doktoritöös läbiviidud uuringute põhilised tulemused ja nende uudsus on järgmine:

✓ Juurutati ja võeti laboratoorsesse kasutusse grafeenoksiidi ja redutseeritud grafeenoksiidi tehnoloogia, mis põhineb loodusliku grafiidi pulbri töötlemisel modifitseeritud mehaano-keemilisele meetodil;

✓ Töötati välja ja võeti kasutusse tehnoloogia õhukeste GO ja RGO liht-, hübriidsete GO+PPy ja submikromeetrilise paksusega komposiitsete rGO/laminaat katete valmistamiseks roostevaba terase ja titaansulami alustele, kasutades lihtkatete tegemiseks vurrkatmise, hübriidsete katete jaoks elektrokeemilise ja komposiitkatete tarvis aatomkihtsadestamise tehnikaid;

✓ GO ja rGO õhukesed lihtkatted näitasid korrosioonikatsetes ja -testides üles piiratud metallipindade kaitse omadusi, mistõttu neid saab kasutada vähekorrodeeruvates ja suhteliselt kuivades keskkondades või siis karmimates tingimustes suhteliselt lühiajaliselt. Igal juhul ei suuda sellised katted kaitsta roostevaba terast punktkorrosiooni eest, kui objekt asub pikemat aega neutraalse pH-ga soolalahuses;

✓ Hübriidsed GO-PPy katted, mis kanti SS-alustele, olid antud töö kõige paksemad katted (~10 µm) ja need näitasid üles keskmist terasaluse kaitset korrosiooni vastu, pidades vastu standardsed 72 tundi reaktiivst immersioonitesti, vastavalt ASTM G48A eeskirjale. Samas, pärast 144 h sama testi oli märgata hübriidkatte purunemist ja aluse pinnalt irdumist, seega katte kaitsefunktsiooni lõppemist. Seetõttu saab väita, et seda tüüpi

katteid on võimalik kasutada pikemat aega keskmiselt reaktiivsetes kesk-kondades. Samuti võib selline kate pakkuda huvi meditsiinilistes kasu-tustes, näiteks implantaatide, proteeside katmiseks, kuna polüpürrool on tuntud biosõbralik materjal ning sellele saab hõlpsasti lisada ravimeid ja/või põletikuvastaseid lisandeid. Kahjuks ei saa sellist hübriidset kaket kasutada pindadel, mis peavad taluma suurt mehaanilist koormust ja/või hõõrdumist, kuna materjal on suhteliselt pehme.

✓ Komposiitkate, mis koosneb üliõhukesest rGO aluskattest ning sellel ALD meetodil sadestatud submikromeetrilise paksusega metalloksiidide laminaadist näitas nii SS- kui Ti5-alustel väga head korrosiooni takis-tavaid omadusi, mida näitasid nii kiired elektrokeemilised mõõtmised/ testid kui ka pikaajalised immersioonitestid (30–40 päeva) soolalahustes. Samas kui ei grafeenil põhinevad lihtkatted, ega ka laminaatkate üksinda ei olnud võimeline kaitsma kumbagi sulami tüüpi – oletatavad põhjused leiavad põhjalikumat käsitlemist dissertatsioonis.

✓ Seega näitasid antud töös valmistatud ja testitud kolm nanografeenil põhinevat erinevat tüüpi kaitsekatet erinevat kaitsevõime taset metallide pindade kaitsmisel korrosiooni vastu, mis lubab neid kasutusele võtta erinevatel kasutusaladel, olenevalt kasutuskeskkonna reaktiivsusest. Saame siiski väita, et väljatöötatud kaitsekatted, kasutatuna sobilikes keskkondades, lubavad tõsta metallobjektide/-detailide ning nendest valmistatud seadmete eluiga, aidates nii kokku hoida materjale ja energiat ning seeläbi luua jätkusuutlikumat ühiskonda.

ACKNOWLEDGEMENTS

As the studies presented in this thesis are done in collaboration, I want to thank all the co-authors for their contribution. I would like to give my heartfelt gratitude to my supervisor Prof. Väino Sammelselg, for his inspiring guidance, constant encouragement and assistance, which enabled me to complete this thesis successfully. I would like to express my gratitude to Prof. Alda Simões, for sharing her valuable expertise, knowledge about Electrochemistry and Electrochemical Impedance of Corrosion, helping to finish this thesis and giving me the opportunity to use her laboratory. I am also very thankful to my lab mates Ms. Jekaterina Kozlova, Mr. Maido Merisalu, Mr. Lauri Aarik, Ms. Andriea Marques, and Ms. Sofia Panao for their help and constant encouragement.

I thank my family for giving me emotional support during the entire time.

RRFERENCES

[1] Shaw BA, Kelly RG. What is corrosion? Interface **(2006)**, 15, 24–26; see also http://www.electrochem.org/dl/interface/spr/spr06/spr06_p24-26.pdf; last accessed: 28.01.2016.

[2] Jones DA. Principals and Prevention of Corrosion, 2nd ed. Prentice Hall: 1996, Upper Saddle River, NJ.

[3] Hays GF, World Corrosion Organization, Corrodia, Fall 2010, see http://events.nace.org/euro/corrodia/Fall_2010/wco.asp; last accessed 28.01.2016.

[4] Schreiber HP, Wertheimer MR, Wrobel AM. Corrosion protection by plasma-polymerized coatings. Thin Solid Films **(1980)**, 72, 487–494; (doi: 10.1016/0040-6090(80)90536-2).

[5] Chou TP, Chandrasekaran C, Limmer SJ, Seraji S, Wu Y. Organic–inorganic hybrid coatings for corrosion protection. Journal of Non-Crystalline Solids **(2001),** 290, 153–162; (doi: 10.1016/S0022-3093(01)00818-3).

[6] Wicks Jr. ZW, Jones FN, Consultant SPP, Wicks. Organic Coatings: Science and Technology, 3rd ed. **(2006)**, John Wiley & Sons, Inc., Hoboken, NJ, USA,**.**

[7] Wang D, Bierwagen GP. Sol–gel coatings on metals for corrosion protection. Prog. Org. Coat. **(2009)**, 64, 327–338; (doi: 10.1016/j.porgcoat.2008.08.010).

[8] Zheng SX, Li JH. Inorganic–organic sol gel hybrid coatings for corrosion protection of metals. J. Sol-Gel Sci. Technol. **(2010)**, 54, 174–187; (DOI: 10.1007/s10971-010-2173-1).

[9] Niinistö L., Ritala M., Leskelä M. Synthesis of oxide thin films and overlayers by atomic layer epitaxy for advanced applications. Mat Sci. and Eng. B – Solid State materials for advanced technology **(1996)**, 41, 23–29; (doi: 10.1016/S0921-5107(96)01617-0).

[10] Tan CK, Blackwood DJ. Corrosion protection by multilayered conducting polymer coatings. Corrosion Science, **(2003)**, 45, 545–557; (doi: 10.1016/S0010-938X(02)00144-0).

[11] Vadukumpully S, Paul J, Mahanta N, Valiyaveettil S. Flexible conductive graphene/poly (vinyl chloride) composite thin films with high mechanical strength and thermal stability. Carbon, **(2011)**, 49, 198–205; (doi: 10.1016/j.carbon.2010.09.004).

[12] Nan HN, Ni ZH, Wang J, Zafar Z, Shi ZX, Wang YY. The thermal stability of graphene in air investigated by Raman spectroscopy. J. Raman Spectrosc. **(2013)**, 44, 1018–1021; (DOI: 10.1002/jrs.4312).

[13] Mattevi C, Eda G, Agnoli S, Miller S, Mkhoyan KA, Celik O, Mastrogiovanni D, Granozzi G, Garfunkel E, Chhowalla M. Evolution of Electrical, Chemical, and Structural Properties of Transparent and Conducting Chemically Derived Graphene Thin Films. Adv. Funct. Mater. **(2009)**, 19, 2577–2583; (DOI: 10.1002/adfm.200900166).

[14] Bunch JS, Verbridge SS, Alden JS, Van der Zande AM, Parpia JM, Craighead HG, McEuen PL. Impermeable Atomic Membranes from Graphene Sheets. Nano Lett. **(2008)**, 8, 2458–2462; (DOI: 10.1021/nl801457b).

[15] Berry V. Impermeability of graphene and its applications. Carbon, **(2013)**, 62, 1–10; (doi: 10.1016/j.carbon.2013.05.052).

[16] Kim KS, Zhao Y, Jang H, Lee SY, Kim JM, Kim KM, Ahn JH, Kim P, Choi JY, Hong BH. Large-scale pattern growth of graphene films for stretchable transparent electrodes. Nature, **(2009)**, 457, 706–710; (DOI: 10.1038/nature07719).

[17] Chen S, Brown L, Levendorf M, Cai W, Ju SY, Edgeworth J, Li X, Magnuson CW, Velamakanni A, Piner RD, Kang J, Park J, Ruoff RS. Oxidation Resistance of Graphene-Coated Cu and Cu/Ni Alloy. ACS Nano, **(2011)**, 5, 1321–1327; (DOI: 10.1021/nn103028d).

[18] Topsakal M, Şahin H, Ciraci S, Graphene coatings: An efficient protection from oxidation. Phys. Rev. B, **(2012)**, 85, 155445; (DOI: 10.1103/ PhysRevB.85.155445).

[19] Kalita G, Ayhan ME, Sharma S, Shinde SM, Ghimire D, Wakita K, Umeno M, Tanemura M. Low temperature deposited graphene by surface wave plasma CVD as effective oxidation resistive barrier. Corros. Sci. **(2014)**, 78, 183–187; (doi: 10.1016/j.corsci.2013.09.013).

[20] Prasai D, Tuberquia JC, Harl RR, Jennings GK, Bolotin KI.Graphene: Corrosion-Inhibiting Coating. ACS Nano, **(2012)**, 6, 1102–1108; (DOI: 10.1021/nn203507y).

[21] Kirkland NT, Schiller T, Medhekar N, Birbilis N. Exploring graphene as a corrosion protection barrier. Corros. Sci. **(2012)**, 56, 1–4; (doi: 10.1016/ j.corsci.2011.12.003).

[22] Dong Y, Liu Q, Zhou Q. Corrosion behavior of Cu during graphene growth by CVD. Corros. Sci. **(2014),** 89 214–219; (DOI: 10.1016/j.corsci.2014.08.026).

[23] Kozlova J, Niilisk A, Alles H, Sammelselg V. Discontinuity and misorientation of graphene grown on nickel foil: Effect of the substrate crystallographic orientation. Carbon, **(2015)**, 94, 160–173; (doi: 10.1016/j.carbon.2015.06.023).

[24] Schriver M, Regan W, Gannett WJ, Zaniewski AM, Crommie MF, Zettl A. Graphene as a Long-Term Metal Oxidation Barrier: Worse Than Nothing. ACS Nano, **(2013)**, 7, 5763–5768; (DOI: 10.1021/nn4014356).

[25] Mondal J, Kozlova J, Sammelselg V. Graphene Nanoplatelets Based Protective and Functionalizing Coating for Stainless Steel. J. Nanosci. Nanotechnol. **(2015),** 15, 6747–6750. (doi: 10.1166/jnn.2015.10775).

[26] Reut J, Öpik A, Idla K. Corrosion behavior of polypyrrole coated mild steel. Synth. Met. (1999), 102, 1392–1393; (doi: 10.1016/S0379-6779(98)01036-4).

[27] Selvaraj M, Palraj S, Maruthan K, Rajagopal G, Venkatachari G. J. Synthesis and characterization of polypyrrole composites for corrosion protection of steel. Appl. Polym. Sci. **(2010)**, 116, 1524–1537; (DOI: 10.1002/app.31430).

[28] Mondal J, Marandi M, Kozlova J, Merisalu M, Niilisk A, Sammelselg V. Protection and Functionalizing of Stainless Steel Surface by Graphene oxide-Polypyrrole Composite Coating. J. Chem. Chem. Eng. **(2014)**, 8 786–793; (doi: 10.17265/ 1934-7375/2014.08.005).

[29] Mondal J, Aarik L, Kozlova J, Niilisk A, Mändar H, Mäeorg U, Simões A, Sammelselg V. Functionalization of Titanium Alloy Surface by Graphene Nanoplatelets and Metal Oxides: Corrosion Inhibition. J. Nanosci. Nanotechnol. **(2015)**, 15, 6533–6540; (DOI: 10.1166/jnn.2015.10775).

[30] Matero R, Ritala M, Leskelä M, Salo M, Aromaa J, Forsen OJ. Atomic layer deposited thin films for corrosion protection. J. Phys. IV France, **(1999)**, 9, 493–499; (DOI: 10.1051/jp4:1999862).

[31] Díaz B, Härkönen E, Swiatowska J, Maurice V, Seyeux A, Marcus P, Ritala M. Low-temperature atomic layer deposition of Al_2O_3 thin coatings for corrosion protection of steel: Surface and electrochemical analysis. Corros. Sci. **(2011)**, 53, 2168–2175; (doi: 10.1016/j.corsci.2011.02.036).

[32] Sammelselg V, Netšipailo I, Aidla A, Tarre A, Aarik L, Asari J, Ritslaid P, Aarik J. Chemical resistance of thin film materials based on metal oxides grown by

atomic layer deposition. Thin Solid Films, **(2013),** 542, 219–224; (doi: 10.1016/ j.tsf.2013.06.079).

[33] Mondal J, Marques A, Aarik L, Kozlova J, Simões A, Sammelselg V. Effect of Graphene Interlayer between Ceramic Anti Corrosion Nanolaminate and Stainless Steel Substrate. Corrosion Science, Available online 14 January 2016 (doi:10.1016/j.corsci.2016.01.013).

[34] Hummers WS, Offeman RE. Preparation of graphitic oxide. J Am Chem Soc. **(1958)**, 80, 1339; (DOI: 10.1021/ja01539a017).

[35] Paredes JI, Rodil SV, Alonso AM, Tascon JMD. Graphene Oxide Dispersions in Organic Solvents. Langmuir, **(2008)**, 24, 10560–10564; (DOI: 10.1021/ la801744a).

[36] Hernandez Y, Nicolosi V, Lotya M, Blighe FM, Sun Z, et.al. JN. High-yield production of graphene by liquid-phase exfoliation of graphite. Nature Nanotech. **(2008)**, 3, 563–568. (DOI: 10.1038/nnano.2008.215).

[37] Kruusenberg I, Mondal J, Matisen L, Sammelselg V, Tammeveski K. Oxygen reduction on graphene-supported MN_4 macrocycles in alkaline media. Electrochem Commun**. (2013)**, 33, 18–22; (doi: 10.1016/j.elecom.2013.04.005).

[38] Fan ZJ, Kai W, Yan J, Wei T, Zhi LJ, Feng J, Ren Y, Song LP, Wei F. Facile Synthesis of Graphene Nanosheets *via* Fe Reduction of Exfoliated Graphite Oxide. ACS Nano, **(2011)**, 5, 191–198; (DOI: 10.1021/nn102339t).

[39] Pham VH, Pham HD, Dang TT, Hur SH, Kim EJ, Kong BS, Kima S, Chung JS. Chemical reduction of an aqueous suspension of graphene oxide by nascent hydrogen. J. Mater. Chem. **(2012)**, 22, 10530–10536; (doi: 10.1039/C2JM30562C)

[40] Aarik J, Aidla A, Kiisler AA, Uustare T, Sammelselg V. Influence of substrate temperature on atomic layer growth and properties of HfO_2 thin films. Thin Solid Films, **(1999)**, 340, 110–116; (DOI: 10.1016/S0040-6090(98)01356-X).

[41] G. J. Brug, A. L. G. Van den Eeden, M. Sluyters-Rehbach, J. H. Sluyters. The analysis of electrode impedances complicated by the presence of a constant phase element. J. Electroanal. Chem. **(1984)**, 176, 275–295; (doi: 10.1016/S0022-0728(84)80324-1).

[42] Zoltowski P. On the electrical capacitance of interfaces exhibiting constant phase element behavior. J. Electroanal. Chem. **(1998)**, 443, 149–154. (doi: 10.1016/ S0022-0728(97)00490-7).

[43] Tuinstra F, Koenig JL. Raman Spectrum of Graphite. J Chem Phys. **(1970)**, 53, 1126. (doi: 10.1063/1.1674108).

[44] Rodil SV, Paredes JI, Alonso MA, Tascón JMD. Preparation of graphene dispersions and graphene-polymer composites in organic media. J Mater Chem. **(2009)**, 19, 3591–3593; (DOI: 10.1039/b904935e).

[45] Ferrari AC, Robertson J. Interpretation of Raman spectra of disordered and amorphous carbon. J Phys Rev B, **(2000),** 61, 14095; (DOI: 10.1103/ PhysRevB.61.14095).

[46] Stankovich S, Dikin DA, Dommett GHB, Kohlhaas KM, Zimmey EJ, Stach EA, Piner RD, Nguyen SBT, Ruoff RS. Graphene-based composite materials. Nature, **(2006)**, 442, 282–286; (DOI: 10.1038/nature04969).

[47] Stankovich S, Piner RD, Chen X, Wu N, Nguyen SBT, Ruoff RS. Stable aqueous dispersions of graphitic nanoplatelets via the reduction of exfoliated graphite oxide in the presence of poly(sodium 4-styrenesulfonate). J Mater Chem. **(2006)**, 16, 155–158; (DOI: 10.1039/B512799H).

[48] Schniepp HC, Li JL, McAllister MJ, Sai H, Herrera-Alonso M, Adamson DH, et al. Functionalized single graphene sheets derived from splitting graphite oxide. J Phys Chem B, **(2006)**, 110, 8535–8539; (DOI: 10.1021/jp060936f).

[49] Park S, An J, Piner RD, Jung I, Yang D, Velamakanni A, Nguyen SBT, Ruoff RS. Aqueous Suspension and Characterization of Chemically Modified Graphene Sheets. Chem Mater. **(2008)**, 20, 6592–6594; (DOI: 10.1021/cm801932u).

[50] Fan X, Peng W, Li Y, Li X, Wang S, Zhang G, Zhang F. Deoxygenation of Exfoliated Graphite Oxide under Alkaline Conditions: A Green Route to Graphene Preparation. Adv Mater. **(2008)**, 20, 4490–4493; (DOI: 10.1002/adma.200801306).

[51] Jung I, Dikin DA, Piner RD, Ruoff RS. Tunable electrical conductivity of individual graphene oxide sheets reduced at "low" temperatures. Nano Lett. **(2008)**, 8, 4283–4287; (DOI: 10.1021/nl8019938).

[52] Szabo T, Berkesi O, Dekany I. DRIFT study of deuterium-exchanged graphite oxide. Carbon, **(2005)**, 43, 3186–3189; (doi: 10.1016/j.carbon.2005.07.013).

[53] Titelman GI, Gelman V, Bron S, Khalfin RL, Y. Cohen, and H. Bianco-Peled. Characteristics and microstructure of aqueous colloidal dispersions of graphite oxide. Carbon, **(2005)**, 43, 641–649; (doi: 10.1016/j.carbon.2004.10.035).

[54] Hontoria-Lucas C, Lopez-Peinado AJ, Lopez-Gonzalez JD, Rojas-Cervantes MJ, Martin-Aranda RM. Study of oxygen-containing groups in series of graphite oxides: physical and chemical characterization. Carbon, **(1995)**, 33, 1585–1592; (doi: 10.1016/0008-6223(95)00120-3).

[55] Stoller MD, Park S, Zhu Y, An A, Ruoff RS. Graphene-Based Ultracapacitors. Nano Lett. **(2008)**, 8, 3498–3502. (DOI: 10.1021/nl802558y).

[56] Jeong HK, Lee YP, Lahaye RJ, Park MH, An KH, Kim IJ, Yang CW, Park CY, Ruoff RS, Lee YH. Evidence of graphitic AB stacking order of graphite oxides. J Am Chem Soc. **(2008)**, 130, 1362–1366; (DOI: 10.1021/ja076473o).

[57] Yan J, Zhao Z, Pan L. Growth and characterization of graphene by chemical reduction of graphene oxide in solution. Phys Status Solidi A, **(2011)**, 208, 2335–2338; (DOI: 10.1002/pssa.201084172).

[58] Prabakar SRJ, Hwang YH, Bae EG, Lee DK, Pyo M. Graphene oxide as a corrosion inhibitor for the aluminum current collector in lithium ion batteries. Carbon, **(2013)**, 52, 128–136; (doi: 10.1016/j.carbon.2012.09.013).

[59] Deng M, Yang X, Silke M, Qiu W, Xu M, Borghs M, Chen H. Electrochemical deposition of polypyrrole/graphene oxide composite on microelectrodes towards tuning the electrochemical properties of neural probes. Sensors and Actuators B: Chemical. **(2011)**, 158, 176–184; (doi: 10.1016/j.snb.2011.05.062).

[60] Wang J, Xu Y, Zhu J, Ren P. Electrochemical in situ polymerization of reduced graphene oxide/polypyrrole composite with high power density. J. Power Sources, **(2012)**, 208, 138–143; (doi:10.1016/j.jpowsour.2012.02.018).

[61] Mikat J, Orgzall I, Hochheimer HD. Raman spectroscopy of conducting polypyrrole under high pressure. Phys. Rev. B, **(2002)**, 65, 174202; (DOI: 10.1103/PhysRevB.65.174202).

[62] Stavaux PY. Effect of Electrolyte Concentration and Nature on the Morphology and the Electrical Properties of Electropolymerized Polypyrrole Nanotubules. Chem. Mater. **(1999)**, 11, 829–834; (DOI: 10.1021/cm9807541).

[63] CaoYQ, Cao ZY, Li X, Wu D, Li AD. A facile way to deposit conformal Al_2O_3 thin film on pristine graphene by atomic layer deposition. Appl. Surf. Sci. **(2013)**, 291, 78–82; (doi: 10.1016/j.apsusc.2013.10.133).

[64] Johns JE, Alaboson JMP, Patwardhan S, Ryder CR, Schatz GC, Hersam MC. Metal Oxide Nanoparticle Growth on Graphene via Chemical Activation with Atomic Oxygen. J Am Chem Soc. **(2013)**, 135, 18121–18125; (DOI: 10.1021/ja408248z).

[65] Aarik J, Aidla A, Kiisler A, Uustare T, Sammelselg V. Effect of crystal structure on optical properties of TiO_2 films grown by atomic layer deposition. Thin Solid Films **(1997)**, 305, 270–273; (doi: 10.1016/S0040-6090(97)00135-1).

[66] Aarik J, Kasikov A, Kirm M, Lange S, Uustare T, Mändar H. Optical properties of crystalline Al_2O_3 thin films grown by atomic layer deposition. Proc. SPIE**, (2005)**, 5946, 594601; (DOI: 10.1117/12.639047).

[67] Alles H, Aarik A, Aidla A, et. al. Atomic layer deposition of HfO_2 on graphene from $HfCl_4$ and H_2O. Central European J. Phys. **(2011)**, 9, 319–324; (DOI: 10.2478/s11534-010-0040-x).

[68] Schedin F, Geim AK, Morozov SV, Hill EW, Blake P, Kats-Nelson MI, Novoselov KS. Detection of individual gas molecules adsorbed on graphene. Nat Mater. **(2007)**, 6, 652–655; (DOI: 10.1038/nmat1967).

[69] Yang Y, Murali R. Binding mechanisms of molecular oxygen and moisture to graphene. Appl Phys Lett. **(2011)**, 98, 093116; (doi: 10.1063/1.3562317).

[70] Jandhyala S, Mordi G, Lee B, Lee G, Floresca C, Cha PR, et. al. Atomic Layer Deposition of Dielectrics on Graphene Using Reversibly Physisorbed Ozone. ACS Nano, **(2012)**, 6, 2722–2730; (DOI**:** 10.1021/nn300167t).

[71] Lin XQ, Ni J, Fang C. Adsorption capacity of H_2O, NH_3, CO, and NO_2 on the pristine graphene. Appl. Phys. **(2013)**, 113, 034306; (doi: 10.1063/1.4776239).

[72] Cavanagh AS, Wilson CA, Weimer AW, George SM. Atomic layer deposition on gram quantities of multi-walled carbon nanotubes. Nanotechnology, **(2009)**, 20, 255602; (DOI: 10.1088/0957-4484/20/25/255602).

[73] Sun X, Xie M, Wang G, Sun H, Cavanagh AS, Travis JJ, George SMJ. Atomic Layer Deposition of TiO_2 on Graphene for Supercapacitors. J Electrochem Soc. **(2012)**, 159, A364–A369; (DOI: 10.1149/2.025204jes).

[74] Burstein GT, Pistorius PC. Surface Roughness and the Metastable Pitting of Stainless Steel in Chloride Solutions. Corrosion, **(1995)**, 51, 380–385; (doi: 10.5006/1.3293603).

[75] Jüttner K. Electrochemical impedance spectroscopy (EIS) of corrosion processes on inhomogeneous surfaces. Electrochim. Acta**, (1990)**, 35, 1501–1508; (doi: 10.1016/0013-4686(90)80004-8).

[76] Boissy C, Alemany-Dumont C, Normand B. EIS evaluation of steady-state characteristic of 316L stainless steel passive film grown in acidic solution. Electrochem. Comm. **(2013)**, 26, 10–12; (doi: 10.1016/j.elecom.2012.09.040).

[77] Huang VMW, Vivier V, Frateur I, Orazem ME, Tribollet B. The Global and Local Impedance Response of a Blocking Disk Electrode with Local Constant-Phase-Element Behavior. J. Electrochem. Soc. **(2007)**, 154, C89–C98; (DOI: 10.1149/1.2398889).

[78] Jorcin JB, Krawiec H, Pébère H, Vignal V. Comparison of local electrochemical impedance measurements derived from bi-electrode and microcapillary techniques. Electrochim. Acta **(2009)**, 54, 5775–5781; (DOI: 10.1016/j.electacta.2009.05.029).

[79] Compton OC, Nguyen SB, Graphene Oxide. Highly Reduced Graphene Oxide, and Graphene: Versatile Building Blocks for Carbon-Based Materials. Small **(2010)**, 6, 711–723; (DOI: 10.1002/smll.200901934).

[80] Liu J, Galpaya D, Notarianni M, Yan C, Motta N. Graphene-based thin film supercapacitor with graphene oxide as dielectric spacer. Appl. Phys. Lett. **(2013)**, 103, 063108; (doi: 10.1063/1.4818337)

[81] Fröhlich K, Rosová A, Dobročka E, Hušeková K, Aarik J, Aidla A. Growth of High-Dielectric-Constant TiO_2 Films in Capacitors with RuO_2 Electrodes. Electrochem. Solid-State Lett. **(2008)**, 11, G19–G21; (DOI: 10.1149/1.2898184).

[82] Gröner MD, Fabreguette FH, Elam JW, George SM. Low-Temperature Al_2O_3 Atomic Layer Deposition. Chem. Mater. **(2004)**, 16, 639–645; (DOI: 10.1021/cm0304546).

[83] Mills D. Electrochemical Methods in Corrosion Research. Corrosion Engineering, Science and Technology **(2007)**, 42, 12–13; (doi: 10.1179/174327807X186673).

[84] Tato W, Landolt D. Electrochemical Determination of the Porosity of Single and Duplex PVD Coatings of Titanium and Titanium Nitride on Brass. J. Electrochem. Soc. **(1998)**, 145, 4173–4181; (DOI: 10.1149/1.1838932).

[85] Liu C, Bi Q, Leyland A, Matthews A. An electrochemical impedance spectroscopy study of the corrosion behaviour of PVD coated steels in 0.5 N NaCl aqueous solution: Part II.: EIS interpretation of corrosion behavior. Corros. Sci. **(2003)**, 45, 1257–1273; (DOI: 10.1016/S0010-938X(02)00214-7).

[86] Ahn SH, Yoo JH, Choi YS, Kim JG, Han JG. Corrosion behavior of PVD-grown WC–$(Ti_{1-x}Al_x)$N films in a 3.5% NaCl solution. Surf. Coat. Technol. **(2003)**, 162, 212–221; (doi: 10.1016/S0257-8972(02)00519-4).

[87] Grips VKW, Selvi VE, Barshilia HC, Rajam KS. Effect of electroless nickel interlayer on the electrochemical behavior of single layer CrN, TiN, TiAlN coatings and nanolayered TiAlN/CrN multilayer coatings prepared by reactive dc magnetron sputtering. Electrochim. Acta **(2006)**, 51, 3461–3468; (doi: 10.1016/j.electacta.2005.09.042).

[88] Díaz B, Swiatowska J, Mauricea V, Seyeux A, Normand B, Härkönen E, Ritala M, Marcus P. Electrochemical and time-of-flight secondary ion mass spectrometry analysis of ultra-thin metal oxide (Al_2O_3 and Ta_2O_5) coatings deposited by atomic layer deposition on stainless steel. Electrochim. Acta, **(2011)**, 56, 10516–10523; (doi: 10.1016/j.electacta.2011.02.074).

[89] Basame SB, White HS. Pitting Corrosion of Titanium The Relationship Between Pitting Potential and Competitive Anion Adsorption at the Oxide Film/Electrolyte Interface. J Electrochem Soc. **(2000)**, 147, 1376–1381; (DOI: 10.1149/1.1393364).

CURRICULUM VITAE

Name: Jay Mondal
Date of birth: 01/03/1988.
Citizenship: Indian
Telephone: +372 58181183
E-mail: jay.mondal0103@gmail.com, jayanta.mondal@ut.ee

Education:
2011–   University of Tartu, Department of Material Science, PhD
               student in Materal Sience;
2008–2010   Indian Institute of Technology Madras, India, master student in
               Chemistry (M.Sc. in Chemistry);
2005–2008   University of Calcutta, Kolkata, India, bachelor student in
               chemistry (B.Sc. in Chemistry);
2003–2005   West Bengal Board of Higher Secondary Education, Kolkata,
               India (Natural Science);
1998–2003   West Bengal Board of Secondary Education, Kolkata, India.

Language skills:
Bengali (Native)
English (Second, writing and speaking well)
Estonian (Basic level)

Research Field:
Material Science and Nanotechnoloy, Surface Coating and Thin Film Technology, Corrosion Science, Surface Science, Advanced Nanostructured Materials

List of basic publications included in the thesis:
1. **J. Mondal**, J. Kozlova, V. Sammelselg. Graphene Nanoplatelets Based Protective and Functionalizing Coating for Stainless Steel, J. Nanosci. Nanotechnol. 2015, **15** (9), 6747–6750.
2. **J. Mondal**, M. Marandi, J. Kozlova, M. Merisalu, A. Niilisk, V. Sammelselg. Protection and Functionalizing of Stainless Steel Surface by Graphene Oxide-Polypyrrole Composite Coating, Journal of Chemistry and Chemical Engineering, 2014, **8**, 786–793.
3. **J. Mondal**, A. Marques, L. Aarik, J. Kozlova, A. Simões, V. Sammelselg. Development of a Ceramic-Graphene nanolaminate coating for corrosion protection of stainless steel Corrosion Sci. 2016 (Available online: 27.01.2016) DOI:10.1016/j.corsci.2016.01.013.
4. **J. Mondal**, L. Aarik, J. Kozlova, A. Niilisk, H. Mändar, U. Mäeorg, A. Simões, V. Sammelselg. Titanium Alloy Corrosion Inhibition by Graphene Nanoplates, J. Nanosci. Nanotechnol. 2015, **15** (9), 6533–6540.

Other publications:
1. Kruusenberg, **J. Mondal**, L. Matisen, V. Sammelselg, K. Tammeveski. Oxygen reduction on graphene-supported MN4 macrocycles in alkaline media, Electrochemistry Communications, 2013, **33**, 18–22.
2. K-K. Türk, I. Kruusenberg, **J. Mondal**, P. Rauwel, J. Kozlova, L. Matisen, V. Sammelselg, K. Tammeveski. Oxygen electroreduction on MN4 macrocycle modified graphene/carbon nanotube composite, Journal of Electroanalytical Chemistry, 2015, **756**, 69–76.
3. H. Kwon, **J. Mondal**, K. AloGab, V. Sammelselg, M. Takamichi, A. Kawaski, K. Kallip, M. Leparoux. Graphene oxide-reinforced aluminum alloy matrix composite materials fabricated by powder metallurgy. (Submitted: Journal of Composite Materials).

Scholarships and honors:
Sept. 2011 – Aug. 2015: Archimedes foundation DoRa scholarship for full time PhD student – Department of Material Science, University of Tartu;
Sept. 2012, Aug. 2013, July 2014 and Sept. 2014: Archimedes foundation DoRa scholarship for short time foreign conference visit, Department of Material Science, University of Tartu;
Sept. 2014 – Dec. 2014: Archimedes foundation DoRa scholarship for foreign university visit, Department of Material Science, University of Tartu.

Other research related contribution (presentations at conferences/symposiums, participation in professional associations/institutions):
GrapHEL (27–30/09/2012, Greece, Mykonos), Preparation and characterization of graphene-polypyrrole nanocomposites and their thin films on different metal surfaces (poster presentation).
E-MRS (27–31/05/2013, France, Strasbourg), Novel anti-corrosion graphene oxide-polypyrrole hybrid coating for 304 stainless steel (poster presentation).
Eurofillers 2013 (25–29/08/2013, Bratislava, Slovakia), Graphene/reduced graphene oxide based anti-corrosion coatings (oral presentation).
Department of Defense Corrosion Conference (16–17/09/2013, Webinar, USA), Anodized aluminium pore sealing with graphene oxide-polypyrrole composite (oral presentation).
Graphene Study 2014 (2–7/02/2014, Obergurgl, Austria), Corrosion protective effect of graphene nanoplates: Study (poster presentation).
International Conference on Advanced Nanomaterials, ANM 2014 (1–4/072014, University of Aveiro, Aveiro, Portugal), Graphene Oxide and Graphene Corrosion Inhibition (oral presentation).
NANOSMAT (8-11/09/2014, Trinity College Dublin, Ireland), Titanium Alloy Corrosion Inhibition by Graphene Nanoplates (oral presentation).

Foreign laboratory visit:
Sept. 2014 – Dec. 2014: University of Lisbon, Instituto Superior Técnico

Hobbies: Travelling, football, volleyball

ELULOOKIRJELDUS

Nimi: Jay Mondal
Sünniaeg: 01/03/1988.
Kodakondsus: India
Telefon: +372 58181183
E-post: jay.mondal0103@gmail.com, jayanta.mondal@ut.ee

Haridus:

2011–	Tartu Ülikool, Materjaliteaduse osakond, materjaliteaduse doktorant;
2008–2010	Indian Institute of Technology Madras, India, keemia magistrant (M.Sc. keemias);
2005–2008	University of Calcutta, Kolkata, India, bakalaureuse üliõpilane keemias (B.Sc. keemias);
2003–2005	West Bengal Board of Higher Secondary Education, Kolkata, India (loodusteadused);
1998–2003	West Bengal Board of Secondary Education, Kolkata, India.

Keelteoskus:
Bengali (emakeel)
Inglise (teine keel, kirjutamise ja kõne tase hea)
Eesti (algtase)

Uurimisvaldkond:
Materjaliteadus ja nanotehnoloogia, pinnakatete valmistamine ja õhukeste tahkiskilede tehnoloogia, korrosiooniteadus, pinnateadus, kõrgtehnoloogilised nanostruktuursed materjalid

Põhipublikatsioonid doktoritöös:
1. **J. Mondal**, J. Kozlova, V. Sammelselg. Graphene Nanoplatelets Based Protective and Functionalizing Coating for Stainless Steel, J. Nanosci. Nanotechnol. 2015, **15** (9), 6747–6750.
2. **J. Mondal**, M. Marandi, J. Kozlova, M. Merisalu, A. Niilisk, V. Sammelselg. Protection and Functionalizing of Stainless Steel Surface by Graphene Oxide-Polypyrrole Composite Coating, Journal of Chemistry and Chemical Engineering, 2014, **8**, 786–793.
3. **J. Mondal**, A. Marques, L. Aarik, J. Kozlova, A. Simões, V. Sammelselg. Development of a Ceramic-Graphene nanolaminate coating for corrosion protection of stainless steel Corrosion Sci. 2016 (Available online: 27.01.2016) DOI:10.1016/j.corsci.2016.01.013.
4. **J. Mondal**, L. Aarik, J. Kozlova, A. Niilisk, H. Mändar, U. Mäeorg, A. Simões, V. Sammelselg. Titanium Alloy Corrosion Inhibition by Graphene Nanoplates, J. Nanosci. Nanotechnol. 2015, **15** (9), 6533–6540.

Publikatsioonid, mis ei ole doktoritööga seotud:
1. Kruusenberg, **J. Mondal**, L. Matisen, V. Sammelselg, K. Tammeveski. Oxygen reduction on graphene-supported MN4 macrocycles in alkaline media, Electrochemistry Communications, 2013, **33**, 18–22.
2. K-K. Türk, I. Kruusenberg, **J. Mondal**, P. Rauwel, J. Kozlova, L. Matisen, V. Sammelselg, K. Tammeveski. Oxygen electroreduction on MN4 macrocycle modified graphene/carbon nanotube composite, Journal of Electroanalytical Chemistry, 2015, **756**, 69–76.
3. H. Kwon, **J. Mondal**, K. AloGab, V. Sammelselg, M. Takamichi, A. Kawaski, K. Kallip, M. Leparoux. Graphene oxide-reinforced aluminum alloy matrix composite materials fabricated by powder metallurgy. (Submitted: Journal of Composite Materials).

Saadud uurimistoetused ja stipendiumid:
Sept. 2011 – Aug. 2015: Archimedes foundation DoRa scholarship for full time PhD student – Department of Material Science, University of Tartu;
Sept. 2012, Aug. 2013, July 2014 and Sept. 2014: Archimedes foundation DoRa scholarship for short time foreign conference visit, Department of Material Science, University of Tartu;
Sept. 2014 – Dec. 2014: Archimedes foundation DoRa scholarship for foreign university visit, Department of Material Science, University of Tartu.

Teised teadustööga seotud tegevused (konverentside ettekanded):
GrapHEL (27–30/09/2012, Greece, Mykonos), Preparation and characterization of graphene-polypyrrole nanocomposites and their thin films on different metal surfaces (poster presentation).
E-MRS (27–31/05/2013, France, Strasbourg), Novel anti-corrosion graphene oxide-polypyrrole hybrid coating for 304 stainless steel (stendiettekanne).
Eurofillers 2013 (25–29/08/2013, Bratislava, Slovakia), Graphene/reduced graphene oxide based anti-corrosion coatings (suuline ettekanne).
Department of Defense Corrosion Conference (16–17/09/2013, Webinar, USA), Anodized aluminium pore sealing with graphene oxide-polypyrrole composite (suuline ettekanne).
Graphene Study 2014 (2–7/02/2014, Obergurgl, Austria), Corrosion protective effect of graphene nanoplates: Study (stendiettekanne).
International Conference on Advanced Nanomaterials, ANM 2014 (1–4/072014, University of Aveiro, Aveiro, Portugal), Graphene Oxide and Graphene Corrosion Inhibition (suuline ettekanne).
NANOSMAT (8-11/09/2014, Trinity College Dublin, Ireland), Titanium Alloy Corrosion Inhibition by Graphene Nanoplates (suuline ettekanne).

Välislaborite külastamine:
Sept. 2014 – dets. 2014: University of Lisbon, Instituto Superior Técnico

Huvialad: Reisimine, jalgpall, võrkpall

DISSERTATIONES SCIENTIAE MATERIALIS
UNIVERSITATIS TARTUENSIS

1. **Martin Järvekülg.** Tubular microstructures by Hf-, Zr- and Ti-butoxide gel sheet rolling. Tartu, 2011, 112 p.
2. **Sergei Vlassov.** Investigation of nanoscale interactions and mechanical properties of nanostructures using quartz tuning fork based real-time measurements. Tartu, 2011, 171 p.
3. **Margus Kodu.** Pulsed Laser Deposition of Magnesium Oxide and Barium Ternary Oxides for Plasma Display Protective Layers. Tartu, 2011, 89 p.
4. **Rainer Pärna.** Surface studies of some oxide films. Tartu, 2011, 129 p.
5. **Jevgeni Šulga**. Self-assembly and interaction of nanostructures. Tartu, 2011, 114 p.
6. **Wojciech Kuznik.** Quantum-chemical computer simulations of the linear and non-linear optical properties of pyrazoloquinoline and dicyanopyrazine derivatives. Tartu, 2012, 89 p.
7. **Leonid Dorogin.** Structural and tribological properties of zero- and one-dimensional nanocrystals. Tartu, 2012, 193 p.
8. **Viljar Palmre.** Fabrication and characterization of microporous carbon-based electroactive polymer actuators. Tartu, 2012, 99 p.
9. **Madis Paalo**. Synthesis of CNT-metal oxide nanocomposites: sol-gel process, rheology, structural and functional properties. Tartu, 2014, 175 p.
10. **Raul Välbe.** Developement of ionic liquid composites by sol-gel method for elaboration of industrial nano- and microstructures. Tartu, 2014, 97 p.
11. **Urmas Joost.** Impurity and preparation dependent properties of titania thin films. Tartu, 2014, 155 p.
12. **Madis Umalas**. Application of sol-gel technology for production of ceramic nanocomposites and functional coatings. Tartu, 2015, 136 p.
13. **Elena Samsonova.** Energy transfer probe as a tool to study morphological and structural origins of fluorescence quenching in rare-earth doped nanophosphors. Tartu, 2015, 114p.